PERGAMON

International Journal of Solids and Structures 40 (2003) 1681–1712

INTERNATIONAL JOURNAL OF SOLIDS and STRUCTURES

www.elsevier.com/locate/ijsolstr

Homogenization of two-phase elasto-plastic composite materials and structures Study of tangent operators, cyclic plasticity and numerical algorithms

I. Doghri *, A. Ouaar

CESAME, Université catholique de Louvain (UCL), Bâtiment Euler, 4 Avenue G., Lemaître, B1348 Louvain-la-Neuve, Belgium

Received 7 March 2002; received in revised form 5 December 2002

Abstract

We develop homogenization schemes and numerical algorithms for two-phase elasto-plastic composite materials and structures. A Hill-type incremental formulation enables the simulation of unloading and cyclic loadings. It also allows to handle any rate-independent model for each phase. We study the crucial issue of tangent operators: elasto-plastic (or "continuum") versus algorithmic (or "consistent"), and anisotropic versus isotropic. We apply two methods of extraction of isotropic tangent moduli. We compare mathematically the stiffnesses of various tangent operators. All rate equations are discretized in time using implicit integration. We implemented two homogenization schemes: Mori–Tanaka and a double inclusion model, and two plasticity models: classical J_2 plasticity and Chaboche's model with non-linear kinematic and isotropic hardenings. We consider composites with different properties and present several discriminating numerical simulations. In many cases, the results are validated against finite element (FE) or experimental data. We integrated our homogenization code into the FE program ABAQUS using a user material interface UMAT. A two-scale procedure allows to compute realistic structures made of non-linear composite materials within reasonable CPU time and memory usage; examples are shown.

Keywords: Composites; Micro-mechanics; Homogenization; Plasticity; Numerical algorithms; Finite elements

1. Introduction

In this paper, we present homogenization models and robust numerical algorithms for two-phase elasto-plastic composites. We use the generic term of "inclusions" to designate the reinforcing phase. The inclusions can be particles, fibers (long or short) or platelets. Actually, all those shapes can be generated by

* Corresponding author. Tel.: +32-10-478042/472350; fax: +32-10-472180.
E-mail addresses: doghri@mema.ucl.ac.be (I. Doghri), ouaar@mema.ucl.ac.be (A. Ouaar).

0020-7683/02/$ - see front matter © 2002 Elsevier Science Ltd. All rights reserved.
doi:10.1016/S0020-7683(03)00013-1

setting appropriate values to the aspect ratio of a spheroid (i.e., an ellipsoid with an axis of revolution). There are many industrial examples of the composites we study in this paper, as illustrated hereafter.

- Polymer matrix composites (PMCs) reinforced with ceramic, glass or Kevlar fibers. Objective: improve stiffness and strength. Examples: boat hulls, aircraft wings, cars (body frames, hood and door panels), sporting equipment.
- Polymer matrix with low modulus rubber particles. Objective: improve toughness and impact resistance. Example: car bumpers.
- Rubber matrix with carbon-black particles. Objective: improve toughness and stiffness. Example: tires.
- Metal matrix composites (MMCs) with ceramic particles or short fibers. Objective: mainly high-temperature applications. Example: fossil-fuel engine components (e.g., turbochargers).
- Concrete matrix with: metallic fibers (strength in tension or bending), polymer or natural fibers (better ductility, lower density), rubber inclusions (impact resistance, acoustic isolation).

In all those cases, we wish to predict the influence of the microstructure on the overall properties of the material or the product. An elegant solution is provided by a micro/macro or two-scale approach with a macro-scale (that of the body) and a micro-scale (the heterogeneous microstructure). In this paper, transition between the two scales is made via average-field theories, also known as homogenization models.

One could use another approach: direct FE computation of the boundary-value problem (BVP) at each representative volume element (RVE). This is feasible for linear elasticity—e.g. (PALMYRA, 2001)—where the problem is reduced to computing a constant macro-stiffness. The method is also very useful for validating homogenization models (as we do in this work) or for studying heterogeneous media with complex material behavior, e.g. (Kouznetsova et al., 2002). However, the direct approach becomes way too expensive if one or more of the following conditions are met: (1) material or geometric non-linearities; (2) non-periodic or complex microstructures (e.g., RVEs containing hundreds of fibers in different orientations); (3) two-scale finite element (FE) simulation of realistic structures (a micro-FE mesh has to be attached to each quadrature point of the macro-mesh). In the latter case, the method requires much more computer power than what is usually available to engineers or researchers.

For elasto-plastic two-phase composites, a good deal of the literature on homogenization revolves around the method proposed in (Tandon and Weng, 1988), a Mori–Tanaka (MT) scheme (Mori and Tanaka, 1973) restricted to J_2 elasto-plasticity with a "secant" (or total) deformation formulation. This precludes the use of other rate-independent models or a simulation of unloading.

Our aim in this work is to develop a formulation and the corresponding numerical algorithms which are able to simulate within reasonable accuracy, computer time and memory: (1) any rate-independent model for either phase; (2) cyclic loadings; (3) any multi-axial stress state; (4) structures made of composite materials.

We address the important issue of tangent operators in elasto-plasticity and their impact on overall predictions in detail. Indeed, we study anisotropic operators ("continuum" and algorithmic), isotropic moduli (computed with two methods) and the relative stiffnesses of those various operators.

Those issues were not studied in the incremental formulation of MT model which was recently proposed in (Pettermann et al., 1999). However, that reference deals with thermal strains and contains several interesting numerical simulations for fiber-reinforced materials, while the simulations presented in this paper are restricted to isothermal conditions and spherical inclusions (validation for other shapes is a work in progress: (Friebel, 2002; Doghri and Friebel, 2003)).

The paper has the following outline. In Section 2 we present some mathematical notation and results which are needed in the remainder of the article. We present anisotropic continuum and consistent tangent operators for two elasto-plastic models (J_2 and Chaboche's cyclic plasticity) in Section 3. We present two methods of extraction of the isotropic part of tangent operators in Section 4. A stiffness comparison of

various tangent operators is carried out in Section 5. We show how to extend homogenization models from linear elasticity to rate-independent non-linear material behavior in Section 6. The MT model and its numerical implementation using implicit algorithms are presented in Section 7, while Section 8 gives similar information for the double inclusion (DI) model. Numerical simulations of three composite materials under various loadings are presented in Section 9. Two-scale numerical simulations of two composite structures are presented in Section 10. Finally, conclusions and directions for future work are discussed in Section 11. In many cases, numerical predictions are compared against FE results or experimental data.

2. Preliminaries

In this section, we define some notations and give some results which are needed later.

Boldface symbols denote tensors, the order of which is indicated by the context. Einstein's summation convention over repeated indices is used unless otherwise indicated:

$$a_{ik}b_{kj} \equiv \sum_{k=1}^{3} a_{ik}b_{kj}$$

Dots and colons are used to indicate tensor products contracted over one and two indices, respectively:

$$\boldsymbol{u}\cdot\boldsymbol{v} = u_i v_i; \quad (\boldsymbol{a}\cdot\boldsymbol{u})_i = a_{ij}u_j;$$
$$(\boldsymbol{a}\cdot\boldsymbol{b})_{ij} = a_{ik}b_{kj}; \quad \boldsymbol{a}:\boldsymbol{b} = a_{ik}b_{ki};$$
$$(\boldsymbol{C}:\boldsymbol{a})_{ij} = C_{ijkl}a_{lk}; \quad (\boldsymbol{C}:\boldsymbol{D})_{ijkl} = C_{ijmn}D_{nmkl}.$$

Tensor products are designated by $\otimes$, e.g.,

$$(\boldsymbol{u}\otimes\boldsymbol{v})_{ij} = u_i v_j; \quad (\boldsymbol{a}\otimes\boldsymbol{b})_{ijkl} = a_{ij}b_{kl}.$$

The symbols $\mathbf{1}$ and $\boldsymbol{I}$ designate the second- and fourth-order symmetric identity tensors, respectively,

$$1_{ij} = \delta_{ij}, \quad I_{ijkl} = \frac{1}{2}(\delta_{ik}\delta_{jl} + \delta_{il}\delta_{jk}), \tag{1}$$

where δ_{ij} is Kronecker's symbol,

$$\delta_{ij} = 1 \text{ if } i = j, \quad \delta_{ij} = 0 \text{ if } i \neq j. \tag{2}$$

The spherical and deviatoric operators are $\boldsymbol{I}^{\mathrm{vol}}$ and $\boldsymbol{I}^{\mathrm{dev}}$, respectively,

$$\boldsymbol{I}^{\mathrm{vol}} \equiv \frac{1}{3}\mathbf{1}\otimes\mathbf{1}, \quad \boldsymbol{I}^{\mathrm{dev}} \equiv \boldsymbol{I} - \boldsymbol{I}^{\mathrm{vol}}, \tag{3}$$

so that for $a_{ij} = a_{ji}$ we have:

$$\boldsymbol{I}^{\mathrm{vol}}:\boldsymbol{a} = \frac{1}{3}a_{mm}\mathbf{1}, \quad \boldsymbol{I}^{\mathrm{dev}}:\boldsymbol{a} = \boldsymbol{a} - \frac{1}{3}a_{mm}\mathbf{1} \equiv \mathrm{dev}(\boldsymbol{a}). \tag{4}$$

Hooke's elasticity operator is designated by $\boldsymbol{c}^{\mathrm{el}}$. In the isotropic case, it is given by

$$\boldsymbol{c}^{\mathrm{el}} = 3\kappa\boldsymbol{I}^{\mathrm{vol}} + 2\mu\boldsymbol{I}^{\mathrm{dev}}, \tag{5}$$

where κ and μ are the elastic bulk and shear moduli, respectively.

For $\boldsymbol{C}$ and $\boldsymbol{D}$ any fourth-order tensors, define the following scalar invariant (Bornert et al., 2001b, p. 178):

$$\boldsymbol{C}::\boldsymbol{D} \equiv C_{ijkl}D_{lkji} = \boldsymbol{D}::\boldsymbol{C}. \tag{6}$$

Using the definition, the following results are easily obtained:

$$\boldsymbol{I}^{\mathrm{vol}} :: \boldsymbol{I}^{\mathrm{vol}} = 1, \quad \boldsymbol{I}^{\mathrm{dev}} :: \boldsymbol{I}^{\mathrm{dev}} = 5, \quad \boldsymbol{I}^{\mathrm{vol}} :: \boldsymbol{I}^{\mathrm{dev}} = 0. \tag{7}$$

Any symmetric and isotropic fourth-order tensor $\boldsymbol{c}^{\mathrm{iso}}$ is a linear combination of $\boldsymbol{I}$ and $(\mathbf{1} \otimes \mathbf{1})$ or, alternatively, of $\boldsymbol{I}^{\mathrm{vol}}$ and $\boldsymbol{I}^{\mathrm{dev}}$. Using the previous results, it is found that $\boldsymbol{c}^{\mathrm{iso}}$ can be written as follows (Bornert et al., 2001b, p. 185):

$$\boldsymbol{c}^{\mathrm{iso}} = (\boldsymbol{I}^{\mathrm{vol}} :: \boldsymbol{c}^{\mathrm{iso}})\boldsymbol{I}^{\mathrm{vol}} + \frac{1}{5}(\boldsymbol{I}^{\mathrm{dev}} :: \boldsymbol{c}^{\mathrm{iso}})\boldsymbol{I}^{\mathrm{dev}}. \tag{8}$$

The notation $\boldsymbol{C}$ "$\geqslant$" $\boldsymbol{D}$ comparing two fourth-order tensors $\boldsymbol{C}$ and $\boldsymbol{D}$ means "*stiffer than*" and is defined as follows:

$$\boldsymbol{C} \text{“}\geqslant\text{”} \boldsymbol{D} \Longleftrightarrow \boldsymbol{a} : \boldsymbol{C} : \boldsymbol{a} \geqslant \boldsymbol{a} : \boldsymbol{D} : \boldsymbol{a}, \quad \forall \boldsymbol{a} \text{ second-order symmetric tensor } (a_{ij} = a_{ji}). \tag{9}$$

In a micro–macro-approach, at each macro-point $\overline{\boldsymbol{x}}$, we know the macro-strain $\overline{\boldsymbol{\epsilon}}(\overline{\boldsymbol{x}})$ and need to compute the macro-stress $\overline{\boldsymbol{\sigma}}(\overline{\boldsymbol{x}})$, or vice-versa. At micro-level, the macro-point is viewed as the center of a RVE with domain ω and boundary $\partial\omega$. It can be shown (e.g., Section 2 in (Nemat-Nasser and Hori, 1999)) that if linear boundary conditions (BCs) are applied to the RVE, then the problem of relating macro-strains and stresses $\overline{\boldsymbol{\epsilon}}$ and $\overline{\boldsymbol{\sigma}}$ can be transformed onto that of relating average strains and stresses $\langle\boldsymbol{\epsilon}\rangle$ and $\langle\boldsymbol{\sigma}\rangle$ over the RVE.

We consider two-phase composites: a number of inclusions (I) in a matrix. The matrix—phase (0)—has volume V_0 and volume fraction $v_0 = V_0/V$, where V is the volume of the RVE. The inclusions—phase (1)—have a total volume $V_1 = \sum_I V_I$ and a volume fraction $v_1 = V_1/V = 1 - v_0$. Define the following volume averages:

$$\langle\boldsymbol{f}\rangle \equiv \frac{1}{V}\int_{\omega} \boldsymbol{f}(\overline{\boldsymbol{x}}, \boldsymbol{x})\,\mathrm{d}V, \quad \langle\boldsymbol{f}\rangle_{\omega_i} \equiv \frac{1}{V_i}\int_{\omega_i} \boldsymbol{f}(\overline{\boldsymbol{x}}, \boldsymbol{x})\,\mathrm{d}V_i, \quad i = 0, 1, \tag{10}$$

where integration is carried out w.r.t. micro-coordinates $\boldsymbol{x}$. In the following, dependence on macro-coordinates $\overline{\boldsymbol{x}}$ will be omitted for simplicity. It is easy to check that the averages over ω (the entire RVE), ω_0 (the matrix phase) and ω_1 (the inclusions phase) are related by

$$\langle\boldsymbol{f}\rangle = v_1\langle\boldsymbol{f}\rangle_{\omega_1} + (1 - v_1)\langle\boldsymbol{f}\rangle_{\omega_0}. \tag{11}$$

The strain averages per phase are related by a strain concentration tensor $\boldsymbol{B}^{\epsilon}$ as follows:

$$\langle\boldsymbol{\epsilon}\rangle_{\omega_1} = \boldsymbol{B}^{\epsilon} : \langle\boldsymbol{\epsilon}\rangle_{\omega_0}. \tag{12}$$

Various homogenization models will differ by the expression of $\boldsymbol{B}^{\epsilon}$. The per-phase average strains are related to the macro-strain $\langle\boldsymbol{\epsilon}\rangle$ by

$$\begin{aligned} \langle\boldsymbol{\epsilon}\rangle_{\omega_0} &= [v_1\boldsymbol{B}^{\epsilon} + (1 - v_1)\boldsymbol{I}]^{-1} : \langle\boldsymbol{\epsilon}\rangle, \\ \langle\boldsymbol{\epsilon}\rangle_{\omega_1} &= \boldsymbol{B}^{\epsilon} : [v_1\boldsymbol{B}^{\epsilon} + (1 - v_1)\boldsymbol{I}]^{-1} : \langle\boldsymbol{\epsilon}\rangle. \end{aligned} \tag{13}$$

Except for the simplest models—Voigt (uniform strain) and Reuss (uniform stress)—the others are based on the fundamental solution of Eshelby (1957). That solution in turn allows to solve the problem of a single ellipsoidal inclusion (I) of uniform moduli $\boldsymbol{c}_1$ which is embedded in an infinite matrix of uniform moduli $\boldsymbol{c}_0$. Under a remote uniform strain $\overline{\boldsymbol{\epsilon}}$ (i.e., linear boundary displacements), it is found (e.g., Chapter 4 in (Mura, 1987), Section 7 in (Nemat-Nasser and Hori, 1999), Chapter 9 in (Lielens, 1999)) that the strain field inside the ellipsoid is uniform and related to the remote (or "macro") strain by

$$\boldsymbol{\epsilon}(\boldsymbol{x}) = \boldsymbol{H}^{\epsilon}(I, \boldsymbol{c}_0, \boldsymbol{c}_1) : \overline{\boldsymbol{\epsilon}} \quad \forall \boldsymbol{x} \in (I), \tag{14}$$

where the single inclusion strain concentration tensor $\boldsymbol{H}^{\epsilon}$ has the following expression:

$$\boldsymbol{H}^{\epsilon}(I,\boldsymbol{c}_0,\boldsymbol{c}_1)=\{\boldsymbol{I}+\mathscr{E}_{(I,\boldsymbol{c}_0)}:[(\boldsymbol{c}_0)^{-1}:\boldsymbol{c}_1-\boldsymbol{I}]\}^{-1}, \tag{15}$$

where $\mathscr{E}(I,\boldsymbol{c}_0)$ is Eshelby's tensor and depends on the geometry of (I) and $\boldsymbol{c}_0$. For a spheroid (I) and an isotropic stiffness $\boldsymbol{c}_0$, $\mathscr{E}$ only depends on the *aspect ratio* and *Poisson's ratio* v (Chapter 2 in (Mura, 1987)). If the moduli are anisotropic, then $\mathscr{E}$ is computed numerically (for that purpose, we used a code which was kindly provided by Lagoudas based on his paper (Gavazzi and Lagoudas, 1990)).

In this paper, we consider two-phase composites where the inclusions (I) have the *same* shape, orientation and stiffness $\boldsymbol{c}_1$ (more general cases are being implemented and tested: (Friebel, 2002; Doghri and Friebel, 2003)). For *any* homogenization model defined by $\boldsymbol{B}^{\epsilon}$—Eq. (12)—the macro-stiffness $\overline{\boldsymbol{c}}$ is given by

$$\overline{\boldsymbol{c}}=[v_1\boldsymbol{c}_1:\boldsymbol{B}^{\epsilon}+(1-v_1)\boldsymbol{c}_0]:[v_1\boldsymbol{B}^{\epsilon}+(1-v_1)\boldsymbol{I}]^{-1}. \tag{16}$$

Finally, for time discretization, the symbol Δ designates an increment over a typical time (or time-like) interval $[t_n,t_{n+1}]$,

$$\Delta(\bullet)\equiv(\bullet)_{n+1}-(\bullet)_n. \tag{17}$$

For simplicity of notation, the subscript $(n+1)$ will be omitted and all variables which do not have this subscript are computed at t_{n+1}.

3. Anisotropic tangent operators

For elasto-plastic materials, one can define at least two tangent operators: a "continuum" and a "consistent" one. Those anisotropic operators can have an important impact on the numerical predictions, because homogenization models depend explicitly on their expressions.

3.1. Continuum and consistent tangent operators

Using the constitutive equations in rate form, it is possible to relate stress and total strain rates as follows:

$$\dot{\boldsymbol{\sigma}}=\boldsymbol{c}^{\mathrm{ep}}:\dot{\boldsymbol{\epsilon}}, \tag{18}$$

where $\boldsymbol{c}^{\mathrm{ep}}$ is called the "continuum" (or elasto-plastic) tangent operator. The "consistent" (or algorithmic) tangent operator is found as follows. First, the rate constitutive equations are discretized in time over each time interval $[t_n,t_{n+1}]$. Next, the algebraic equations thus found are differentiated w.r.t. all the variables at t_{n+1} and the variations of stress and total strain are related as follows:

$$\delta\boldsymbol{\sigma}_{n+1}=\boldsymbol{c}^{\mathrm{alg}}:\delta\boldsymbol{\epsilon}_{n+1}. \tag{19}$$

Designating by (Δp) the plastic multiplier increment, it is found that:

$$\boldsymbol{c}^{\mathrm{alg}}\to\boldsymbol{c}^{\mathrm{ep}}\quad\text{if }\Delta p\to 0,$$

but otherwise $\boldsymbol{c}^{\mathrm{alg}}$ and $\boldsymbol{c}^{\mathrm{ep}}$ can be quite different. In the context of macro-elasto-plasticity, Simo and Taylor (1985) have shown that if the global equilibrium equations are solved using Newton's method, then a quadratic rate of convergence is achieved when using $\boldsymbol{c}^{\mathrm{alg}}$ instead of $\boldsymbol{c}^{\mathrm{ep}}$.

In this paper, we show in Section 5 another result, that is that the elasto-plastic tangent operator $\boldsymbol{c}^{\mathrm{ep}}$ is *stiffer* than the algorithmic tangent $\boldsymbol{c}^{\mathrm{alg}}$. This result can have an impact on homogenization results as will be seen in Section 9.1.

3.2. J_2 elasto-plasticity

The constitutive equations for classical J_2 elasto-plasticity are:

$$\begin{aligned}&\boldsymbol{\sigma} = \boldsymbol{c}^{\mathrm{el}} : (\boldsymbol{\epsilon} - \boldsymbol{\epsilon}^p), \quad f = \sigma_{\mathrm{eq}} - R(p) - \sigma_{\mathrm{Y}} \leqslant 0,\\ &\dot{\boldsymbol{\epsilon}}^p = \dot{p}\boldsymbol{N},\ \dot{p} \geqslant 0,\ \dot{p}f = 0,\ \dot{p}\dot{f} = 0, \quad \boldsymbol{N} = \frac{\partial f}{\partial \boldsymbol{\sigma}} = \frac{3}{2}\frac{\mathrm{dev}(\boldsymbol{\sigma})}{\sigma_{\mathrm{eq}}},\end{aligned} \tag{20}$$

where $\sigma_{\mathrm{Y}} > 0$ is the initial yield stress, $p \geqslant 0$ the accumulated plastic strain, $R(p) \geqslant 0$ the hardening stress, $\sigma_{\mathrm{eq}} \geqslant 0$ the von Mises measure of $\boldsymbol{\sigma}$ and $\boldsymbol{N}$ the normal to the yield surface in stress space. The "continuum" tangent is given by (Section 12.7 in (Doghri, 2000)):

$$\boldsymbol{c}^{\mathrm{ep}} = \boldsymbol{c}^{\mathrm{el}} - \frac{(2\mu)^2}{h}\boldsymbol{N}\otimes\boldsymbol{N}, \quad h = 3\mu + \underbrace{\frac{\mathrm{d}R}{\mathrm{d}p}}_{R'(p)} > 0. \tag{21}$$

The "consistent" moduli are given by (Section 12.10.3 in (Doghri, 2000))

$$\boldsymbol{c}^{\mathrm{alg}} = \boldsymbol{c}^{\mathrm{ep}} - (2\mu)^2(\Delta p)\frac{\sigma_{\mathrm{eq}}}{\sigma_{\mathrm{eq}}^{\mathrm{tr}}}\frac{\partial \boldsymbol{N}}{\partial \boldsymbol{\sigma}}, \quad \frac{\partial \boldsymbol{N}}{\partial \boldsymbol{\sigma}} = \frac{1}{\sigma_{\mathrm{eq}}}\left(\frac{3}{2}\boldsymbol{I}^{\mathrm{dev}} - \boldsymbol{N}\otimes\boldsymbol{N}\right), \tag{22}$$

with $\sigma_{\mathrm{eq}}^{\mathrm{tr}}$ a trial (elastic predictor) value of σ_{eq}. Note that although the constitutive model is isotropic, both tensors $\boldsymbol{c}^{\mathrm{ep}}$ and $\boldsymbol{c}^{\mathrm{alg}}$ are *anisotropic*.

3.3. Chaboche's cyclic plasticity model

We now consider an elasto-plastic model with non-linear kinematic and isotropic hardenings which is successful in predicting cyclic plasticity of metals, including the Baushinger effect. The model was initially proposed by Armstrong and Frederick (1966) and later developed and made popular by Chaboche (see Chapter 5 in (Lemaitre and Chaboche, 1998)). The constitutive equations are:

$$\begin{aligned}&\boldsymbol{\sigma} = \boldsymbol{c}^{\mathrm{el}} : (\boldsymbol{\epsilon} - \boldsymbol{\epsilon}^p), \quad f = \beta_{\mathrm{eq}} - R(p) - \sigma_{\mathrm{Y}} \leqslant 0,\\ &\dot{\boldsymbol{\epsilon}}^p = \dot{p}\boldsymbol{N}, \quad \dot{\boldsymbol{X}} = a\dot{\boldsymbol{\epsilon}}^p - b\boldsymbol{X}\dot{p},\\ &\dot{p} \geqslant 0,\ \dot{p}f = 0,\ \dot{p}\dot{f} = 0, \quad \boldsymbol{N} = \frac{\partial f}{\partial \boldsymbol{\sigma}} = \frac{3}{2}\frac{\boldsymbol{\beta}}{\beta_{\mathrm{eq}}},\end{aligned} \tag{23}$$

where $a > 0$ and $b \geqslant 0$ are kinematic hardening parameters, $\boldsymbol{X}$ is a back stress (kinematic hardening), $\boldsymbol{\beta} \equiv \mathrm{dev}(\boldsymbol{\sigma}) - \boldsymbol{X}$ and β_{eq} the von Mises measure of $\boldsymbol{\beta}$.

The "continuum" (or elasto-plastic) tangent is given by (Doghri, 1993)

$$\boldsymbol{c}^{\mathrm{ep}} = \boldsymbol{c}^{\mathrm{el}} - \frac{(2\mu)^2}{h}\boldsymbol{N}\otimes\boldsymbol{N}, \quad h = 3\mu + R'(p) + \frac{3}{2}a - b\boldsymbol{N} : \boldsymbol{X}. \tag{24}$$

The consistent (algorithmic) tangent operator is given by (Doghri, 1993)

$$\boldsymbol{c}^{\mathrm{alg}} = \boldsymbol{c}^{\mathrm{mod}} - \frac{(\Delta p)(2\mu)^2}{[1+(3/2)g]}\frac{\partial \boldsymbol{N}}{\partial \boldsymbol{\beta}} - \frac{(\Delta p)(2\mu)^2}{[1+(3/2)g]} \times \frac{b}{(1+b\Delta p)^2}\frac{1}{\beta_{\mathrm{eq}}}\frac{1}{h^{\mathrm{alg}}}\left[\frac{3}{2}\boldsymbol{X}_n - (\boldsymbol{N} : \boldsymbol{X}_n)\boldsymbol{N}\right]\otimes\boldsymbol{N}, \tag{25}$$

where $\boldsymbol{c}^{\mathrm{mod}}$ is the "modified" continuum tangent operator:

$$\begin{aligned}
&\boldsymbol{c}^{\mathrm{mod}} = \boldsymbol{c}^{\mathrm{el}} - \frac{(2\mu)^2}{h^{\mathrm{alg}}}\boldsymbol{N}\otimes\boldsymbol{N},\\
&h^{\mathrm{alg}} \equiv 3\mu + R'(p) + \frac{1}{(1+b\Delta p)^2}\left(\frac{3}{2}a - b\boldsymbol{N}:\boldsymbol{X}_n\right),\\
&g \equiv \left(2\mu + \frac{a}{1+b\Delta p}\right)\frac{\Delta p}{\beta_{\mathrm{eq}}}.
\end{aligned} \tag{26}$$

Again, both tangent operators $\boldsymbol{c}^{\mathrm{ep}}$ and $\boldsymbol{c}^{\mathrm{alg}}$ are anisotropic.

4. Isotropic part of tangent operators

Numerical experience has shown that good predictions are obtained only when *Eshelby's tensor* is computed not with an anisotropic tangent operator ($\boldsymbol{c}^{\mathrm{alg}}$ or $\boldsymbol{c}^{\mathrm{ep}}$) but with *isotropic moduli* ($\boldsymbol{c}^{\mathrm{iso}}$). The general expression of the latter is (by design) form-similar to that of Hooke's operator in isotropic linear elasticity:

$$\boldsymbol{c}^{\mathrm{iso}} = 3\kappa_t\boldsymbol{I}^{\mathrm{vol}} + 2\mu_t\boldsymbol{I}^{\mathrm{dev}}, \tag{27}$$

where κ_t and μ_t are "tangent" bulk and shear moduli, resp. Moreover, for a spheroid and isotropic moduli, Eshelby's tensor only needs the "tangent" Poisson's ratio ν_t:

$$\nu_t = \frac{3\kappa_t - 2\mu_t}{2(3\kappa_t + \mu_t)} \tag{28}$$

The way in which an isotropic part ($\boldsymbol{c}^{\mathrm{iso}}$) is extracted from an anisotropic operator ($\boldsymbol{c}^{\mathrm{ani}}$) is *not* unique; we present hereafter two methods which we tried successfully.

4.1. First method: spectral decomposition

This first method applies to anisotropic tangent operators which are a linear combination of I^{vol}, I^{dev} and $(\boldsymbol{N}\otimes\boldsymbol{N})$, where $\boldsymbol{N}$ is typically a normal to a yield surface in stress space and satisfies:

$$N_{ij} = N_{ji}, \quad N_{mm} = 0, \quad \boldsymbol{N}:\boldsymbol{N} = \frac{3}{2}. \tag{29}$$

For J_2 plasticity, both tensors $\boldsymbol{c}^{\mathrm{ep}}$ and $\boldsymbol{c}^{\mathrm{alg}}$ satisfy all conditions. For Chaboche's cyclic plasticity model, the conditions apply to $\boldsymbol{c}^{\mathrm{ep}}$ in all cases and to $\boldsymbol{c}^{\mathrm{alg}}$ only when $b = 0$ (linear kinematic hardening). For those anisotropic operators $\boldsymbol{c}^{\mathrm{ani}}$, Ponte Castañeda (1996) proposes to re-write them as follows:

$$\boldsymbol{c}^{\mathrm{ani}} = 3k_1\boldsymbol{C}^{(1)} + 2k_2\boldsymbol{C}^{(2)} + 2k_3\boldsymbol{C}^{(3)}, \tag{30}$$

where

$$\boldsymbol{C}^{(1)} = \boldsymbol{I}^{\mathrm{vol}}, \quad \boldsymbol{C}^{(3)} = \frac{2}{3}\boldsymbol{N}\otimes\boldsymbol{N}, \quad \boldsymbol{C}^{(2)} = \boldsymbol{I}^{\mathrm{dev}} - \boldsymbol{C}^{(3)}. \tag{31}$$

Those tensors satisfy the following conditions:

$$\boldsymbol{C}^{(1)} + \boldsymbol{C}^{(2)} + \boldsymbol{C}^{(3)} = \boldsymbol{I}, \quad \boldsymbol{C}^{(i)}:\boldsymbol{C}^{(j)} = \delta_{ij}\boldsymbol{C}^{(i)} \text{ (no sum over } i). \tag{32}$$

This is why Eq. (30) is known as a *spectral decomposition* of $\boldsymbol{c}^{\mathrm{ani}}$. A basic assumption in the method is the following:

$$\mathrm{dev}(\Delta\boldsymbol{\epsilon}) \text{ is collinear with } \boldsymbol{N}. \tag{33}$$

It is found then that the incremental stress–strain relation $\Delta\boldsymbol{\sigma} \approx \boldsymbol{c}^{\text{ani}} : \Delta\boldsymbol{\epsilon}$ reduces to $\Delta\boldsymbol{\sigma} \approx \boldsymbol{c}^{\text{iso}} : \Delta\boldsymbol{\epsilon}$, where $\boldsymbol{c}^{\text{iso}}$ is an isotropic operator defined by

$$\kappa_t = k_1, \quad \mu_t = k_3. \tag{34}$$

An application to algorithmic moduli $\boldsymbol{c}^{\text{alg}}$ of J_2 plasticity gives:

$$\kappa_t = \kappa, \quad \mu_t = \mu\left[1 - \frac{3\mu}{h}\right], \quad k_2 = \mu\left[1 - 3\mu\frac{\Delta p}{\sigma_{\text{eq}}^{\text{tr}}}\right]. \tag{35}$$

There are some comments to be made. First, the k_2 term disappeared from $\boldsymbol{c}^{\text{iso}}$ and (Δp) with it, therefore any advantage of consistent vs. continuum tangent is lost. Second, the basic assumption (33) may lead to bad results for non-proportional loadings. Finally, for Chaboche's model, when $b \neq 0$, $\boldsymbol{c}^{\text{alg}}$ is such that Eq. (30) does *not* apply, and using only the other assumption of the method—Eq. (33)—does *not* give an isotropic operator.

4.2. Second method: a general definition

This second method is much more general than the first one and can be applied to any anisotropic operator $\boldsymbol{c}^{\text{ani}}$ (even if it does not represent material moduli). By analogy with decomposition (8)—which is exact for isotropic operators—it is suggested to *define* an isotropic part $\boldsymbol{c}^{\text{iso}}$ of $\boldsymbol{c}^{\text{ani}}$ as follows (Bornert et al., 2001a, p. 194):

$$\boldsymbol{c}^{\text{iso}} \equiv (\boldsymbol{I}^{\text{vol}} :: \boldsymbol{c}^{\text{ani}})\boldsymbol{I}^{\text{vol}} + \frac{1}{5}(\boldsymbol{I}^{\text{dev}} :: \boldsymbol{c}^{\text{ani}})\boldsymbol{I}^{\text{dev}}. \tag{36}$$

This definition can be coded as an independent module which acts as a post-processor for any constitutive box, without knowledge of the particular model or code that the box contains. Indeed, one can check the following expressions:

$$\begin{aligned} \boldsymbol{I}^{\text{vol}} :: \boldsymbol{c}^{\text{ani}} &= 3\kappa_t = \frac{1}{3}c^{\text{ani}}_{lljj}, \\ \boldsymbol{I}^{\text{dev}} :: \boldsymbol{c}^{\text{ani}} &= 10\mu_t = c^{\text{ani}}_{illi} - \frac{1}{3}c^{\text{ani}}_{lljj}. \end{aligned} \tag{37}$$

An application to moduli $\boldsymbol{c}^{\text{alg}}$ of J_2 plasticity gives:

$$\kappa_t = \kappa, \quad \mu_t = \mu - \frac{3}{5}\mu^2\left[\frac{1}{h} + 4\frac{\Delta p}{\sigma_{\text{eq}}^{\text{tr}}}\right]. \tag{38}$$

The expression of μ_t is *different* from that found with the first method, Eq. (35). However, our experience so far has shown that using one definition or the other does not have a significant impact on homogenization results.

For Chaboche's cyclic plasticity model, the isotropic part of $\boldsymbol{c}^{\text{alg}}$ is determined by its tangent moduli as follows:

$$\kappa_t = \kappa, \quad \mu_t = \mu - \frac{3}{5}\mu^2\left[\frac{1}{h^{\text{alg}}} + 4\frac{\Delta p}{\beta_{\text{eq}}}\frac{1}{1 + (3/2)g}\right]. \tag{39}$$

Note that with this second method, μ_t is a function of the plasticity increment Δp, and therefore the isotropic parts of the consistent and continuum tangent operators are different, even for J_2 elasto-plasticity.

5. Stiffness comparison of various tangent operators

We shall see in Section 9.1 that evaluating Eshelby's tensor with anisotropic ($\boldsymbol{c}^{\mathrm{ep}}$ or $\boldsymbol{c}^{\mathrm{alg}}$) or isotropic ($\boldsymbol{c}^{\mathrm{iso}}$) tangent operators has a major impact on homogenization results. This might be traced back to the relative stiffnesses of those operators. Therefore, in this section we set up to prove the following inequalities for J_2 plasticity:

$$\boldsymbol{c}^{\mathrm{el}} \text{“} \geqslant \text{”} \boldsymbol{c}^{\mathrm{ep}} \text{“} \geqslant \text{”} \boldsymbol{c}^{\mathrm{alg}} \text{“} \geqslant \text{”} \boldsymbol{c}^{\mathrm{iso}}, \tag{40}$$

where the symbol “ $\geqslant$ ” means “*stiffer than*” and is defined in Eq. (9). The first inequality ($\boldsymbol{c}^{\mathrm{el}} \text{“} \geqslant \text{”} \boldsymbol{c}^{\mathrm{ep}}$) just translates the experimental fact that the elastic stiffness is larger than any elasto-plastic tangent; it implies that $h > 0$ (see Section 12.7 in (Doghri, 2000)).

We now prove the second inequality ($\boldsymbol{c}^{\mathrm{ep}} \text{“} \geqslant \text{”} \boldsymbol{c}^{\mathrm{alg}}$). From Sections 3.2 and 4.1, it is found that ($\boldsymbol{\eta}$ designating any second-order symmetric tensor):

$$\boldsymbol{\eta} : (\boldsymbol{c}^{\mathrm{ep}} - \boldsymbol{c}^{\mathrm{alg}}) : \boldsymbol{\eta} = \left(6\mu^2 \frac{\Delta p}{\sigma_{\mathrm{eq}}^{\mathrm{tr}}}\right)(\boldsymbol{\eta} : \boldsymbol{C}^{(2)} : \boldsymbol{\eta}) \tag{41}$$

This is the product of two terms, the first of which is always positive. As for the second term, introducing the following decomposition,

$$\mathrm{dev}(\boldsymbol{\eta}) = k\boldsymbol{N} + \boldsymbol{\eta}^{\perp} \tag{42}$$

it can be checked that:

$$\boldsymbol{\eta} : \boldsymbol{C}^{(2)} : \boldsymbol{\eta} = \boldsymbol{\eta}^{\perp} : \boldsymbol{C}^{(2)} : \boldsymbol{\eta}^{\perp}. \tag{43}$$

Using the expressions of $\boldsymbol{C}^{(2)}$, $\boldsymbol{c}^{\mathrm{el}}$ and $\boldsymbol{c}^{\mathrm{ep}}$, it is found that:

$$\boldsymbol{\eta}^{\perp} : \boldsymbol{C}^{(2)} : \boldsymbol{\eta}^{\perp} = \frac{1}{2\mu}\boldsymbol{\eta}^{\perp} : \left[\boldsymbol{c}^{\mathrm{el}} - \left(1 + \frac{R'(p)}{3\mu}\right)(\boldsymbol{c}^{\mathrm{el}} - \boldsymbol{c}^{\mathrm{ep}})\right] : \boldsymbol{\eta}^{\perp}. \tag{44}$$

In practice, $|R'(p)|/(3\mu) \ll 1$, therefore the final result is:

$$\boldsymbol{\eta} : (\boldsymbol{c}^{\mathrm{ep}} - \boldsymbol{c}^{\mathrm{alg}}) : \boldsymbol{\eta} \approx \left(3\mu \frac{\Delta p}{\sigma_{\mathrm{eq}}^{\mathrm{tr}}}\right)(\boldsymbol{\eta}^{\perp} : \boldsymbol{c}^{\mathrm{ep}} : \boldsymbol{\eta}^{\perp}), \tag{45}$$

where the first term is always positive, and the second also for a strain-hardening material (no softening). Therefore we proved that $\boldsymbol{c}^{\mathrm{ep}}$ is *stiffer than* $\boldsymbol{c}^{\mathrm{alg}}$.

We now prove the last inequality ($\boldsymbol{c}^{\mathrm{alg}} \text{“} \geqslant \text{”} \boldsymbol{c}^{\mathrm{iso}}$). Using results from Sections 3.2 and 4.1, it is found that:

$$\boldsymbol{\eta} : (\boldsymbol{c}^{\mathrm{alg}} - \boldsymbol{c}^{\mathrm{iso}}) : \boldsymbol{\eta} = (6\mu^2)\left(\frac{1}{h} - \frac{\Delta p}{\sigma_{\mathrm{eq}}^{\mathrm{tr}}}\right)(\boldsymbol{\eta} : \boldsymbol{C}^{(2)} : \boldsymbol{\eta}). \tag{46}$$

In this product of three scalar factors, we have already proven that the last factor is positive. As for the second factor, it can be rewritten as follows using Eq. (21)b:

$$\frac{1}{h} - \frac{\Delta p}{\sigma_{\mathrm{eq}}^{\mathrm{tr}}} = \frac{(\sigma_{\mathrm{eq}}^{\mathrm{tr}} - 3\mu\Delta p) - R'(p)\Delta p}{h\sigma_{\mathrm{eq}}^{\mathrm{tr}}}. \tag{47}$$

The denominator is positive (since $h > 0$ and $\sigma_{\mathrm{eq}}^{\mathrm{tr}} > 0$). As for the numerator, the return mapping algorithm used to update the constitutive solution (Section 12.10.2 of (Doghri, 2000)) allows to find the following expression:

$$(\sigma_{\text{eq}}^{\text{tr}} - 3\mu\Delta p) - R'(p)\Delta p = \sigma_{\text{Y}} + R(p) - R'(p)\Delta p. \tag{48}$$

Now a first-order Taylor expansion of $R(p)$ around p_n gives

$$R(p) \approx R(p_n) + (\Delta p)R'(p_n). \tag{49}$$

Consequently, we obtain:

$$\sigma_{\text{Y}} + R(p) - R'(p)\Delta p \approx \sigma_{\text{Y}} + R(p_n) + (\Delta p)[R'(p_n) - R'(p)] > 0. \tag{50}$$

This is a sum of positive scalars because σ_{Y}, $R(p_n)$ and Δp are all positive and $R'(p_n) > R'(p)$ from experimental evidence. Therefore, we proved that $\boldsymbol{c}^{\text{alg}}$ is *stiffer* than $\boldsymbol{c}^{\text{iso}}$.

6. Incremental formulation of homogenization models

6.1. Reference moduli

An extension of homogenization models from linear elasticity to rate-independent non-linear behavior (e.g, elasto-plasticity, non-linear elasticity, etc.) is provided by Hill's so-called incremental formulation (Hill, 1965). Indeed, stress and strain rates are related by: $\dot{\boldsymbol{\sigma}} = \boldsymbol{c} : \dot{\boldsymbol{\epsilon}}$, which is form-similar to linear elasticity except that we are using rates and a tangent operator $\boldsymbol{c}$ which should *not* be confused with Hooke's operator $\boldsymbol{c}^{\text{el}}$. Moreover, $\boldsymbol{c}$ will *not* be uniform, because at any time t, it depends on the state of strain or stress. For history-dependent models, it also depends on internal variables and has different expressions according to loading or unloading. Therefore, in the matrix of a composite we have:

$$\dot{\boldsymbol{\sigma}}(\boldsymbol{x}, t) = \boldsymbol{c}_0(\boldsymbol{\epsilon}(\boldsymbol{x}, t), t) : \dot{\boldsymbol{\epsilon}}(\boldsymbol{x}, t) \quad \forall \boldsymbol{x} \in \omega_0.$$

Consequently, it does *not* make sense for instance to evaluate Eshelby's tensor $\mathscr{E}$ using $\boldsymbol{c}_0(\boldsymbol{x}, t)$. A work around is to consider a fictitious *reference* matrix which has *uniform* tangent moduli $\hat{\boldsymbol{c}}_0(t)$:

$$\dot{\boldsymbol{\sigma}}(\boldsymbol{x}, t) = \hat{\boldsymbol{c}}_0(t) : \dot{\boldsymbol{\epsilon}}(\boldsymbol{x}, t) \quad \forall \boldsymbol{x} \in \omega_0. \tag{51}$$

The difficult question of course is how to define the reference material and relate $\hat{\boldsymbol{c}}_0(t)$ to the real composite. Tandon and Weng (1988) developed a *secant* (or total deformation) formulation of MT model in which *average* strains in the matrix phase are used to compute the response of a reference material. This approach was followed by many researchers in the field. So similarly, in our *incremental* formulation of MT, the constitutive box of the real material in each phase is called with the *average* strains and strain rates in that phase, and the moduli that the box computes are taken as the reference moduli for that phase. However, our formulation and implementation are generic and modular enough to allow other reference moduli to be used in the future as long as they are computable and the final numerical results agree reasonably well with experimental data or FE simulations.

There is no unique definition for a reference material, and there is still active research in this subject (e.g., see (Bornert et al., 2001b; Suquet, 1997; Ponte Castañeda and Suquet, 1998, 2001) and references therein). However, the suggestions which are available so far in the literature are either valid for a total deformation theory (which precludes unloading) or hard-wired to J_2 elasto-plasticity or are too complex to implement efficiently.

In Section 9.2 (Fig. 6) there is a comparison between our results and those obtained by Suquet's model in which a reference material is defined by taking the phase-average of the second moments of the stress.

6.2. Time discretization

Rate relations such as the rate version of (12) are discretized over a time interval $[t_n, t_{n+1}]$ as follows:

$$\langle \Delta\boldsymbol{\epsilon} \rangle_{\omega_1} = \boldsymbol{B}^{\epsilon}_{n+\alpha} : \langle \Delta\boldsymbol{\epsilon} \rangle_{\omega_0},$$

where a generalized mid-point rule is used:

$$(\bullet)_{n+\alpha} = (\bullet)_{(t=t_{n+\alpha})}, \quad t_{n+\alpha} = (1-\alpha)t_n + \alpha t_{n+1}, \quad \alpha \in [0,1]. \tag{52}$$

Explicit and implicit integrations correspond to $\alpha = 0$ and $\alpha > 0$, respectively, with special cases: $\alpha = 1$ (backward Euler) and $\alpha = 1/2$ (mid-point rule). In this paper, good predictions were obtained with $\alpha = 1/2$ (in most cases) or $\alpha = 2/3$ (which sometimes allows to take larger time increments for a given accuracy).

6.3. Tangent operators

In Sections 7.2 and 8.2, it is important to notice that *only Eshelby's tensor is computed with the isotropic part of the reference moduli, all other computations are performed with the anisotropic algorithmic moduli.* This insures a good convergence of the whole procedure, i.e.: (i) the homogenization algorithms (Sections 7.2 and 8.2), (ii) the algorithm for macro-stress constraints (Section 6.4) and (iii) the FE computations at macro-scale (Section 10).

6.4. Macro-stress constraints

Macro-stress constraints are handled as in Section D.2 of (Doghri, 2000). Assume for instance that we need to simulate a macro-tension/compression test in the one-direction. In this case, at each time t_{n+1}, $\overline{\epsilon}_{11}$ is known but $\overline{\epsilon}_{22}$ and $\overline{\epsilon}_{33}$ need to be computed from the following conditions:

$$\overline{\sigma}_{22}(\overline{\epsilon}_{22}, \overline{\epsilon}_{33}) = 0, \quad \overline{\sigma}_{33}(\overline{\epsilon}_{22}, \overline{\epsilon}_{33}) = 0. \tag{53}$$

This is a system of two non-linear scalar equations, which is solved iteratively using Newton's method. For each iteration (m), we have:

$$\overline{\sigma}^{(m)}_{ii} + \overline{c}^{(m)}_{ii22}\left(\overline{\epsilon}^{(m+1)}_{22} - \overline{\epsilon}^{(m)}_{22}\right) + \overline{c}^{(m)}_{ii33}\left(\overline{\epsilon}^{(m+1)}_{33} - \overline{\epsilon}^{(m)}_{33}\right) = 0, \text{ no sum, } ii = 22, 33. \tag{54}$$

Convergence is achieved if $|\overline{\sigma}_{22}|$ and $|\overline{\sigma}_{33}|$ are smaller than a tolerance. This means that there is an outer loop around the homogenization algorithms of Sections 7.2 and 8.2 which for each time interval $[t_n, t_{n+1}]$ and each iteration (m) passes macro-strain values $\overline{\epsilon}^{(m)}_{ij}$.

7. Mori–Tanaka model

7.1. Formulation

The MT model was proposed by Mori and Tanaka (1973) and is such that the strain concentration tensor—Eq. (12)—has the following expression (see also Chapter 9 in (Lielens, 1999)):

$$\boldsymbol{B}^{\epsilon} = \boldsymbol{H}^{\epsilon}(I, \boldsymbol{c}_0, \boldsymbol{c}_1), \tag{55}$$

where operator $\boldsymbol{H}^{\epsilon}$ is that of the single inclusion problem, Eq. (15). Consequently, Benveniste (1987) has proposed the following useful interpretation of the MT model: each inclusion (I) behaves like an isolated inclusion in the matrix seeing $\langle \boldsymbol{\epsilon} \rangle_{\omega_0}$ as a far-field strain. The incremental extension of MT to non-linear rate-independent models gives:

$$\langle \dot{\boldsymbol{\epsilon}} \rangle_{\omega_1} = \boldsymbol{H}^{\epsilon}_{(I, \dot{\boldsymbol{c}}_0, \dot{\boldsymbol{c}}_1)} : \langle \dot{\boldsymbol{\epsilon}} \rangle_{\omega_0}. \tag{56}$$

Benveniste's interpretation of this result would be that each inclusion (I) behaves like an isolated inclusion in the reference matrix seeing $\langle\dot{\boldsymbol{\epsilon}}\rangle_{\omega_0}$ as a far-field strain rate. The macro-tangent moduli $\overline{\boldsymbol{c}}$ in MT model will be found as follows:

$$\begin{aligned}&\langle\dot{\boldsymbol{\sigma}}\rangle = \overline{\boldsymbol{c}} : \langle\dot{\boldsymbol{\epsilon}}\rangle,\\ &\overline{\boldsymbol{c}} = \left[v_1\hat{\boldsymbol{c}}_1 : \boldsymbol{H}^{\epsilon}_{(I,\hat{\boldsymbol{c}}_0,\hat{\boldsymbol{c}}_1)} + (1-v_1)\hat{\boldsymbol{c}}_0\right] : \left[v_1\boldsymbol{H}^{\epsilon}_{(I,\hat{\boldsymbol{c}}_0,\hat{\boldsymbol{c}}_1)} + (1-v_1)\boldsymbol{I}\right]^{-1}.\end{aligned} \tag{57}$$

7.2. Numerical implementation

Consider a time interval $[t_n, t_{n+1}]$. The data are: macro-total strains $\overline{\boldsymbol{\epsilon}_n}$ and $\Delta\overline{\boldsymbol{\epsilon}}$, and history variables at t_n. The problem is to compute macro-stress $\overline{\boldsymbol{\sigma}}$ and macro-tangent moduli $\overline{\boldsymbol{c}}$.

- Initialization: $\langle\Delta\boldsymbol{\epsilon}\rangle_{\omega_1} \leftarrow \Delta\overline{\boldsymbol{\epsilon}}$.
- Iterations (i) (upper index (i) omitted for simplicity):
  1. Call constitutive box of real inclusions material with average strains in the inclusions phase $\langle\boldsymbol{\epsilon}_n\rangle_{\omega_1}$ and $\langle\Delta\boldsymbol{\epsilon}\rangle_{\omega_1}$ as arguments. Take the algorithmic (and anisotropic) moduli $\hat{\boldsymbol{c}}_1$ that the box returns as reference moduli for the inclusions phase.
  2. Compute average strain in matrix phase:

     $$\langle\Delta\boldsymbol{\epsilon}\rangle_{\omega_0} = \frac{\Delta\overline{\boldsymbol{\epsilon}} - v_1\langle\Delta\boldsymbol{\epsilon}\rangle_{\omega_1}}{1-v_1}.$$

  3. Call constitutive box of real matrix material with average strains in the matrix phase $\langle\boldsymbol{\epsilon}_n\rangle_{\omega_0}$ and $\langle\Delta\boldsymbol{\epsilon}\rangle_{\omega_0}$ as arguments. Take the algorithmic (and anisotropic) moduli $\hat{\boldsymbol{c}}_0$ that the box returns as reference moduli for the matrix phase.
  4. Extract isotropic part $\hat{\boldsymbol{c}}_0^{\text{iso}}$ from reference matrix moduli $\hat{\boldsymbol{c}}_0$.
  5. Compute Eshelby's tensor with those isotropic moduli: $\mathscr{E}(I, \hat{\boldsymbol{c}}_0^{\text{iso}})$.
  6. Compute values at $t_{n+\alpha}$ of the anisotropic moduli $\hat{\boldsymbol{c}}_0$ and $\hat{\boldsymbol{c}}_1$:

     $$\hat{\boldsymbol{c}}_{r_{(n+\alpha)}} = (1-\alpha)\hat{\boldsymbol{c}}_{r_{(n)}} + \alpha\hat{\boldsymbol{c}}_r; \quad r = 0, 1; \quad \alpha \in]0, 1]$$

     (Our experience so far showed that robust and accurate numerical simulations are obtained with $\alpha = 1/2$ (mid-point rule) or $\alpha = 2/3$.)
  7. Compute strain concentration tensor

     $$\boldsymbol{B}^{\epsilon} = \{\boldsymbol{I} + \mathscr{E} : [(\hat{\boldsymbol{c}}_{0_{(n+\alpha)}})^{-1} : \hat{\boldsymbol{c}}_{1_{(n+\alpha)}} - \boldsymbol{I}]\}^{-1}.$$

  8. Check compatibility of average strain in inclusions phase by computing residual:

     $$\boldsymbol{R} = \boldsymbol{B}^{\epsilon} : [v_1\boldsymbol{B}^{\epsilon} + (1-v_1)\boldsymbol{I}]^{-1} : \Delta\overline{\boldsymbol{\epsilon}} - \langle\Delta\boldsymbol{\epsilon}\rangle_{\omega_1}.$$

  9. If $|\boldsymbol{R}| \leqslant \text{TOL}$, then exit the loop.
  10. Else: new iteration (go to step 1) with new $\langle\Delta\boldsymbol{\epsilon}\rangle_{\omega_1}$:

      $$\langle\Delta\boldsymbol{\epsilon}\rangle_{\omega_1} \leftarrow \langle\Delta\boldsymbol{\epsilon}\rangle_{\omega_1} + \xi\boldsymbol{R}; \quad \xi \in]0, 1]$$

      (ξ is a line search parameter; all the numerical simulations that we ran so far used a value of $\xi = 1$.)
- After convergence, compute macro-moduli $\overline{\boldsymbol{c}}_{n+\alpha}$ and macro-stress increment $\Delta\overline{\boldsymbol{\sigma}}$:

  $$\overline{\boldsymbol{c}}_{n+\alpha} = [v_1\hat{\boldsymbol{c}}_{1_{(n+\alpha)}} : \boldsymbol{B}^{\epsilon} + (1-v_1)\hat{\boldsymbol{c}}_{0_{(n+\alpha)}}] : [v_1\boldsymbol{B}^{\epsilon} + (1-v_1)\boldsymbol{I}]^{-1},$$

  $$\Delta\overline{\boldsymbol{\sigma}} = \overline{\boldsymbol{c}}_{(n+\alpha)} : \Delta\overline{\boldsymbol{\epsilon}}.$$

8. Double inclusion model

8.1. Formulation

The DI model was proposed by Nemat-Nasser and Hori (1999, Section 10)—see also Chapter 9 in (Lielens, 1999)—and supposes that each spheroidal inclusion (I)—of stiffness $\boldsymbol{c}_1$—is wrapped with a hollow inclusion (I_0) of stiffness $\boldsymbol{c}_0$. The outer material has a stiffness $\boldsymbol{c}_R$. Inclusions (I) and (I_0) have the same aspect ratio, symmetry axis and center, and their volume ratio equals that of inclusions and matrix in the actual composite (v_1/v_0).

By changing the stiffness $\boldsymbol{c}_R$ of the outer material, one can retrieve many homogenization models. The choice $\boldsymbol{c}_R = \overline{\boldsymbol{c}}$ gives the self-consistent model. A second choice is $\boldsymbol{c}_R = \boldsymbol{c}_0$, the stiffness of the real matrix material. In this case, it can be shown that the strain concentration tensor—Eq. (12)—is given by

$$\boldsymbol{B}^{\epsilon} = \boldsymbol{H}^{\epsilon}(I, \boldsymbol{c}_0, \boldsymbol{c}_1) \equiv \boldsymbol{B}^{\epsilon}_{l}, \tag{58}$$

i.e., the MT model. A third choice is $\boldsymbol{c}_R = \boldsymbol{c}_1$, the stiffness of the real inclusions (I). In this case, it is found that:

$$\boldsymbol{B}^{\epsilon} = \left[\boldsymbol{H}^{\epsilon}(I, \boldsymbol{c}_1, \boldsymbol{c}_0)\right]^{-1} \equiv \boldsymbol{B}^{\epsilon}_{u}, \tag{59}$$

and this can be called the inverse MT model, as it corresponds to MT for a composite where the material properties of the inclusions and the matrix are permutated. It can be shown that $\boldsymbol{B}^{\epsilon}_{\mathrm{l}}$ and $\boldsymbol{B}^{\epsilon}_{\mathrm{u}}$ correspond to lower and upper stiffness estimates, respectively, which are closely related to the Hashin–Shtrikman bounds (Hashin and Shtrikman, 1963). Consequently, Lielens (Chapter 9 in (Lielens, 1999)) proposed a homogenization model which is based on the following *interpolation*:

$$\boldsymbol{B}^{\epsilon} = \left[(1 - \zeta(v_1))(\boldsymbol{B}^{\epsilon}_{l})^{-1} + \zeta(v_1)(\boldsymbol{B}^{\epsilon}_{u})^{-1}\right]^{-1}, \tag{60}$$

where $\zeta(v_1)$ is a smooth interpolation function which satisfies:

$$\zeta(v_1) > 0, \quad \frac{\mathrm{d}\zeta}{\mathrm{d}v_1}(v_1) > 0, \quad \lim_{v_1 \to 0} \zeta(v_1) = 0, \quad \lim_{v_1 \to 1} \zeta(v_1) = 1. \tag{61}$$

Lielens proposed the following expression for $\zeta(v_1)$:

$$\zeta(v_1) = \frac{1}{2} v_1 (1 + v_1). \tag{62}$$

In the remainder of the paper, "DI" means Lielens' interpolation model thus defined.

8.2. Numerical implementation

The implementation of DI model is very similar to that of MT, and the *only* changes in the algorithm of Section 7.2 are in steps 4, 5 and 7 which now become as follows:

4. Extract isotropic parts $\hat{\boldsymbol{c}}_0^{\mathrm{iso}}$ and $\hat{\boldsymbol{c}}_1^{\mathrm{iso}}$ from reference moduli of the matrix and inclusions, $\hat{\boldsymbol{c}}_0$ and $\hat{\boldsymbol{c}}_1$, respectively.
5. Compute Eshelby's tensors with those isotropic moduli:

$$\mathscr{E}_0 \equiv \mathscr{E}(I, \hat{\boldsymbol{c}}_0^{\mathrm{iso}}), \quad \mathscr{E}_1 \equiv \mathscr{E}(I, \hat{\boldsymbol{c}}_1^{\mathrm{iso}}).$$

7. Compute strain concentration tensors:

$$\boldsymbol{B}^{\epsilon}_{1} = \left\{\boldsymbol{I} + \mathscr{E}_0 : \left[(\hat{\boldsymbol{c}}_{0_{(n+\alpha)}})^{-1} : \hat{\boldsymbol{c}}_{1_{(n+\alpha)}} - \boldsymbol{I}\right]\right\}^{-1},$$

$$\boldsymbol{B}^{\epsilon}_{\mathrm{u}} = \boldsymbol{I} + \mathscr{E}_1 : [(\hat{\boldsymbol{c}}_{1_{(n+\alpha)}})^{-1} : \hat{\boldsymbol{c}}_{0_{(n+\alpha)}} - \boldsymbol{I}],$$

$$\boldsymbol{B}^{\epsilon} = [(1-\zeta(v_1))(\boldsymbol{B}^{\epsilon}_{1})^{-1} + \zeta(v_1)(\boldsymbol{B}^{\epsilon}_{\mathrm{u}})^{-1}]^{-1}.$$

9. Numerical simulations of RVEs

We developed a code called DIGIMAT (for "Digital Materials") in which we implemented two homogenization schemes: MT and DI and two material models: J_2 elasto-plasticity and Chaboche's cyclic plasticity. Those models can be used for any phase of a composite material. The inclusions can be spheres or spheroids with any aspect ratio. All RVE simulations with DIGIMAT reported in this paper took less than 1 s of CPU time on an ordinary PC. For validation purposes, we conducted direct FE computations on a unit cell using ABAQUS (2001)—see Appendix A.

9.1. Time-integration and tangent operators

Figs. 1–3 show numerical simulations with MT of macro-tension tests under imposed macro-strain for a MMC with a J_2 elasto-plastic matrix and $v_1 = 20\%$ of elastic spherical inclusions (complete material data are given in Section 9.2). Figs. 1 and 2 are obtained with Eshelby's tensor computed with tangent moduli $\hat{\boldsymbol{c}}_0^{\mathrm{alg}}$ for two values of the integration parameter: $\alpha = 1$ (backward Euler) in Fig. 1 and $\alpha = 1/2$ (mid-point rule) in Fig. 2. It is seen that in the latter case, the results are insensitive to the value of the macro-strain increment. Fig. 3 compares the results obtained using Eshelby's tensor computed with the anisotropic tangent moduli $\hat{\boldsymbol{c}}_0^{\mathrm{ep}}$ (elasto-plastic) or $\hat{\boldsymbol{c}}_0^{\mathrm{alg}}$ (algorithmic) to those obtained from FE computation. It is seen that the overall response is much stiffer than it should. However, Fig. 3 shows that if *Eshelby's tensor* is

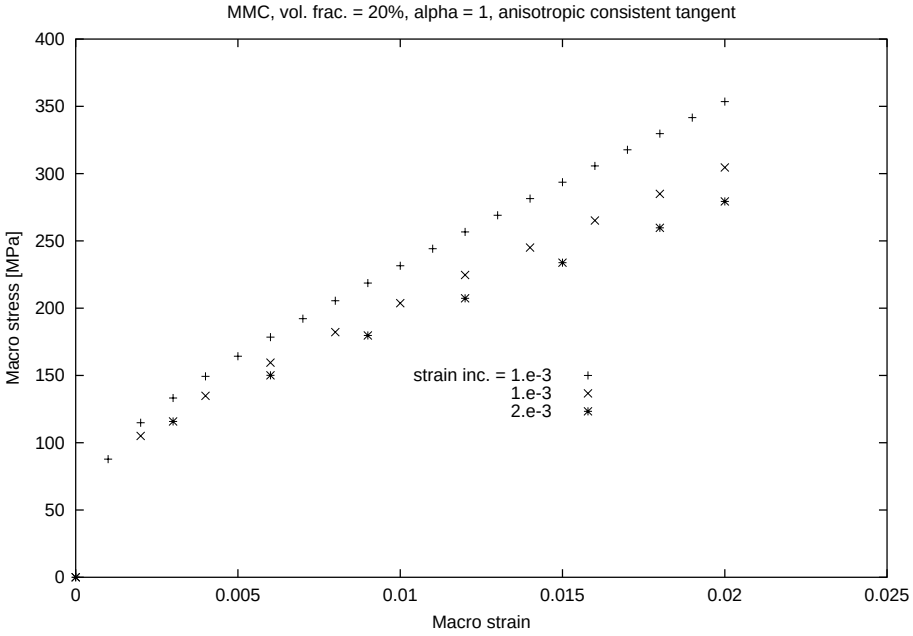

Fig. 1. MMC ($v_1 = 20\%$) under tension. MT results when $\alpha = 1$ and Eshelby's tensor is computed with anisotropic consistent tangent.

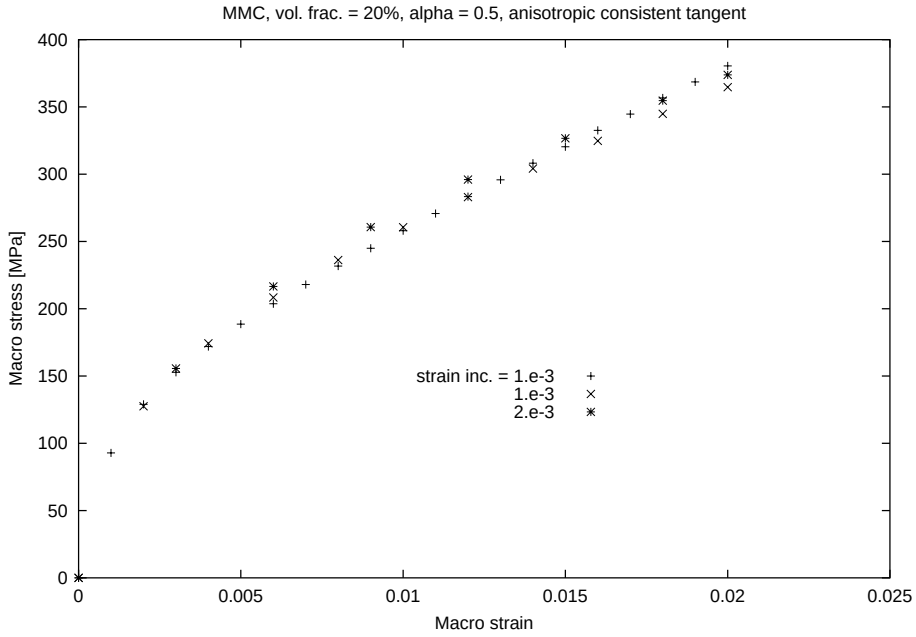

Fig. 2. MMC ($v_1 = 20\%$) under tension. MT results when $\alpha = 0.5$ and Eshelby's tensor is computed with anisotropic consistent tangent.

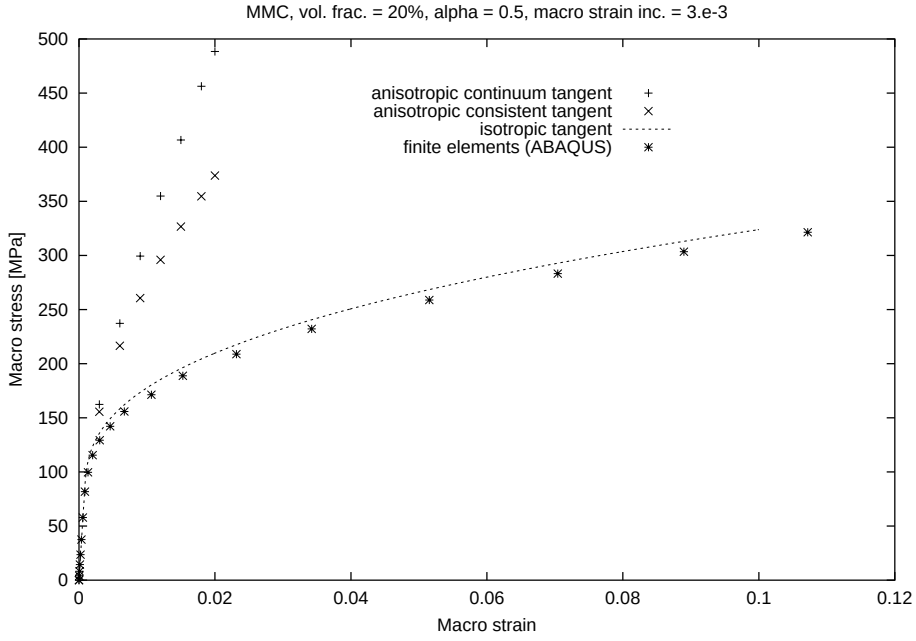

Fig. 3. MMC ($v_1 = 20\%$) under tension. MT results when $\alpha = 0.5$ and Eshelby's tensor is computed with: (1) anisotropic continuum tangent, (2) anisotropic consistent tangent and (3) isotropic tangent. Comparison with target FE unit cell results.

computed with an *isotropic part* of $\hat{\boldsymbol{c}}_0^{\text{alg}}$, then a good agreement with FE results is found. Those facts have already been recorded in the literature (e.g., Bornert et al., 2001b; Gonzalez and Llorca, 2000; Masson et al., 2000; Ponte Castañeda and Suquet, 2001; Suquet, 1997 and references therein), but there is still no satisfying explanation for neither the problem nor the work around. It is difficult to tackle this problem because the overall stiffness is a non-linear function of the strain concentration tensor, which itself is a non-linear function of Eshelby's tensor, and the latter can only be computed numerically if the moduli are anisotropic.

Our contribution to this issue is the following. We proved in Section 5 that $\hat{\boldsymbol{c}}_0^{\text{ep}} \text{“} \geqslant \text{”} \hat{\boldsymbol{c}}_0^{\text{alg}} \text{“} \geqslant \text{”} \hat{\boldsymbol{c}}_0^{\text{iso}}$, and it is seen from Fig. 3 that the predictions of the overall response follow the exact same order. So there is perhaps a link that one could establish mathematically in the future.

Note that *from now on*, all elasto-plastic results which are reported in the following sections and figures were obtained under the following conditions: algorithmic (consistent) tangent operators are used everywhere except in Eshelby's tensor which is computed with an isotropic part of the tangent; time-integration parameter is either $\alpha = 1/2$ (in most cases) or $\alpha = 2/3$ (for PMC, this sometimes allows to use larger time increments without loss in accuracy).

9.2. A metal matrix composite

A metallic matrix (aluminum alloy) has the following properties: $E_0 = 75$ GPa, $v_0 = 0.3$, $\sigma_Y = 75$ MPa, with power-law isotropic hardening ($R(p) = kp^m$) with $k = 416$ MPa and $m = 0.3895$. The matrix is reinforced with spherical ceramic inclusions ($E_1 = 400$ GPa, $v_1 = 0.2$) of volume fraction v_1. This MMC has also been studied by Suquet (1997, p. 254), Gonzalez and Llorca (2000) and Segurado et al. (2002).

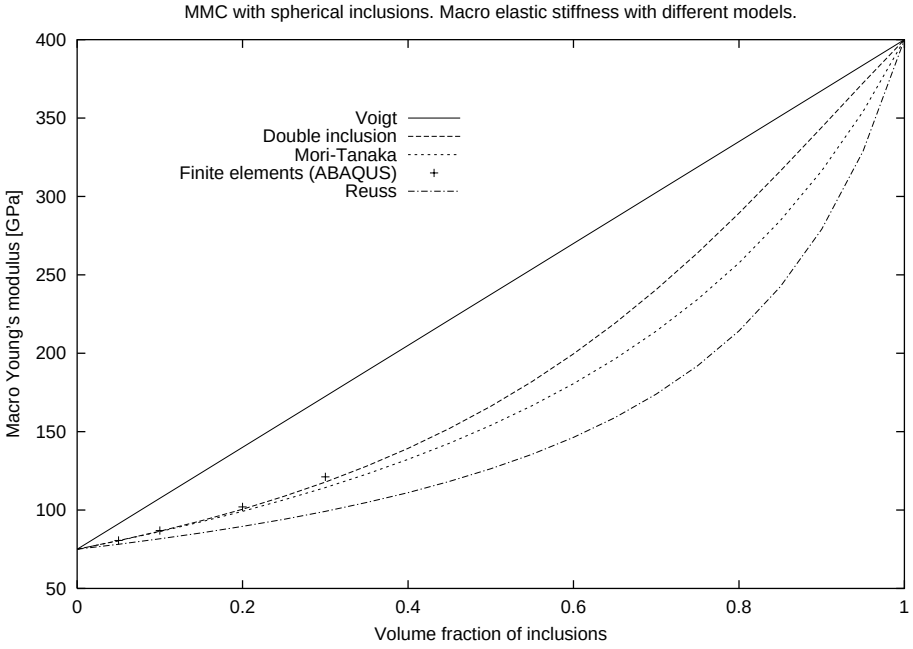

Fig. 4. MMC: macro-Young's modulus predictions with different models: (1) Voigt (uniform strain), (2) double inclusion, (3) Mori–Tanaka, (4) finite elements (unit cell) and (5) Reuss (uniform stress).

Fig. 4 shows predictions of macro-Young's modulus obtained with various homogenization models and with direct FE computations on a unit cell. Both MT and DI give excellent predictions, although the latter performs better for higher values of v_1. Note that in Figs. 4 and 10, values of v_1 higher than the maximum packing concentration $(v_1)_{\max}$ are not physically meaningful. For spherical inclusions of uniform size, $(v_1)_{\max} \approx 0.75$.

Fig. 5 shows numerical simulations with MT of macro-tension tests with imposed macro-strain for various values of v_1. The same tests were simulated with direct FE computations and the results are also shown in Fig. 5. There is good agreement between the two sets of results.

The same MMC under tension was simulated in (Segurado et al., 2002) for $v_1 = 30\%$ using several formulations and the results are plotted in Fig. 6 together with ours. The target results (label 2) were obtained in (Segurado et al., 2002) by performing 3D FE computations on a cube containing 30 spheres. A typical mesh had about 60,000 elements and 90,000 nodes. Twelve meshes were generated corresponding to different arrangements of the spheres and BCs; the average response is plotted (label 2). Results obtained with our incremental MT formulation are plotted with label 1 and those found with a secant (total-deformation) formulation of MT have label 3. Finally, results with label 4 were obtained using a formulation proposed by Suquet (1997) in which reference materials are defined by taking the phase-averages of the second-order moments of the stress. It was shown that this approach is equivalent to Ponte Castañeda's variational formulation (Suquet, 1997; Ponte Castañeda, 1996; Ponte Castañeda and Suquet, 1998, 2001).

Comparison between the target results (label 2) and the others shows that our predictions (label 1) overestimate the non-linear entry but then as hardening develops, they become very close to the target. On the other hand, predictions with Suquet's formulation (label 4), match the non-linear curvature closer but diverge from the target as the strains increase. Finally, the classical secant formulation (label 3) overestimates the stresses at all levels of plastic strains.

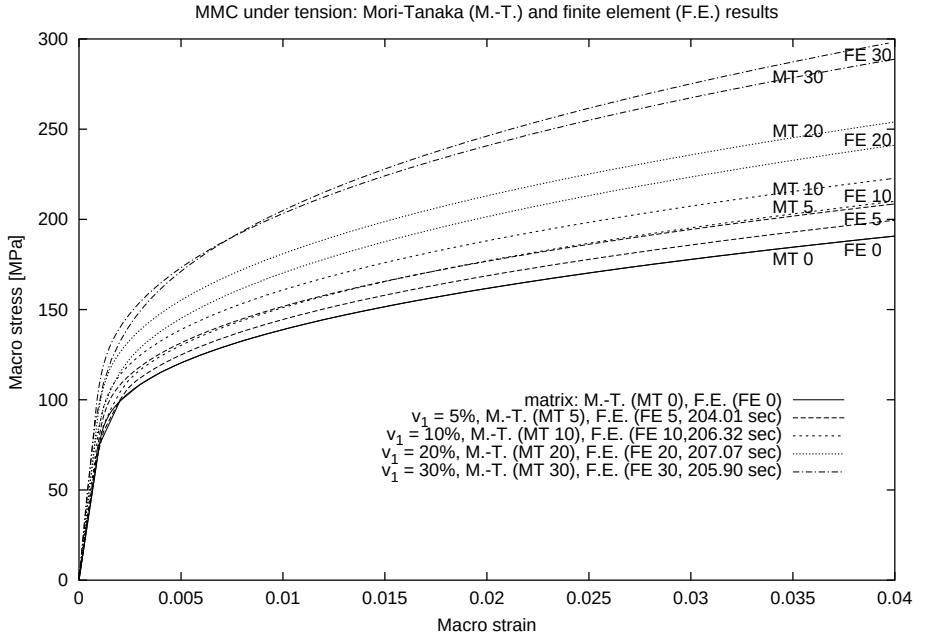

Fig. 5. MMC under macro-tension. Comparaison between MT and unit cell FE predictions for various volume fractions of inclusions v_1.

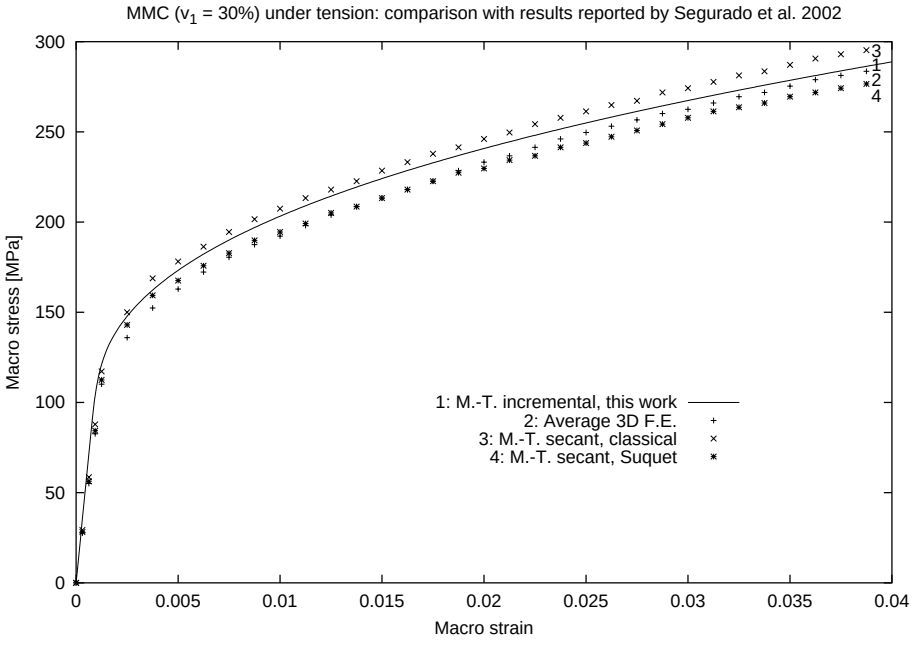

Fig. 6. MMC ($v_1 = 30\%$) under macro-tension. Comparaison of different predictions: (1) incremental MT (this work), (2) average 3D FEs (Segurado et al., 2002), (3) classical secant MT and (4) secant MT with (Suquet, 1997).

In conclusion, it appears that our incremental MT formulation gives acceptable predictions and that the accuracy increases with hardening.

In Fig. 7, for $v_1 = 30\%$, a cyclic tension/compression test under imposed macro-strain (peak values: $\pm 4\%$) is simulated with three methods: MT, DI and FE. It is seen that the two homogenization models perform remarkably well, with MT doing better in the first monotonic stage, and DI giving a closer agreement with FE afterwards. We have done similar simulations for all other values of v_1 and the conclusions are the same. It is important to notice that our incremental formulation allows to simulate cyclic plasticity while a secant formulation does *not*.

In order to further illustrate the robustness of our algorithms, we simulate macro-shear tests in Fig. 8 and macro-bi-axial plane stress loads in Fig. 9. In the latter case, the initial yield envelope is plotted, and it was defined as follows. Proportional macro-strain histories $\overline{\epsilon}_{11}(t)$ and $\overline{\epsilon}_{22}(t)$ are imposed such that their ratio is constant ($\overline{\epsilon}_{33}(t)$ is computed by our DIGIMAT code so that $\overline{\sigma}_{33}(t) = 0$). When the macro-stress ratio $\overline{\sigma}_{11}(t)/\overline{\sigma}_{22}(t)$ is no longer constant, than initial macro-yield is predicted (this criterion is probably too strong).

9.3. A polymer matrix composite

A polymer matrix (epoxy) has the following properties: $E_0 = 3.16$ GPa, $v_0 = 0.35$, $\sigma_Y = 75.86$ MPa, and power-law isotropic hardening with $k = 32.18$ MPa and $m = 0.26$. The properties of the reinforcing spherical elastic inclusions (in silica) are $E_1 = 73.1$ GPa and $v_1 = 0.18$. This composite was studied by Tandon and Weng (1988) who used a secant (total deformation) theory; experimental results are also reported in that reference.

Fig. 10 shows predictions of macro-Young's modulus obtained with various homogenization models and with FE computations. It is seen that the DI model gives excellent agreement with FE, and that the

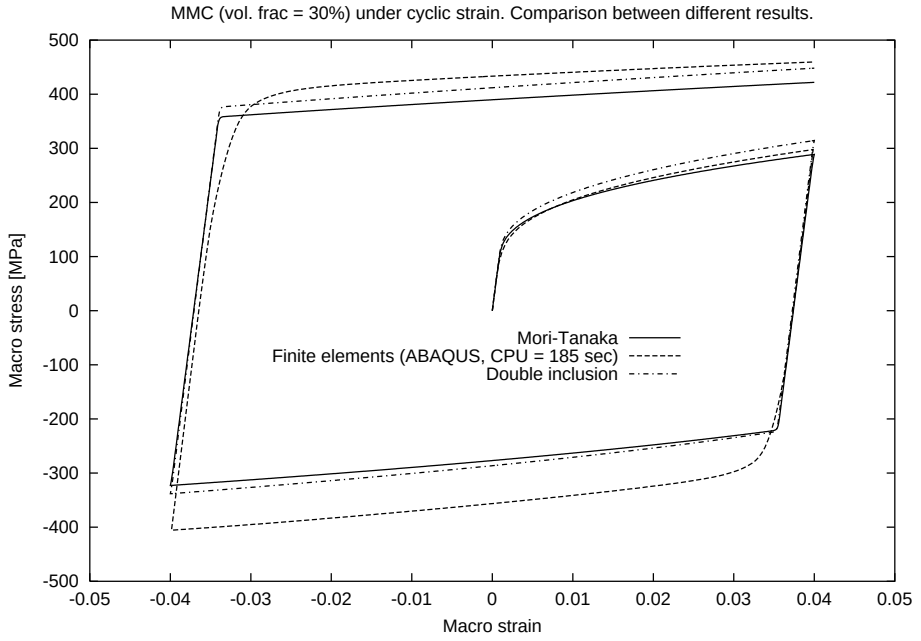

Fig. 7. MMC ($v_1 = 30\%$) under cyclic macro-strain (macro-uniaxial stress). Comparaison of different predictions: (1) MT model, (2) finite elements (unit cell) and (3) interpolative double inclusion model.

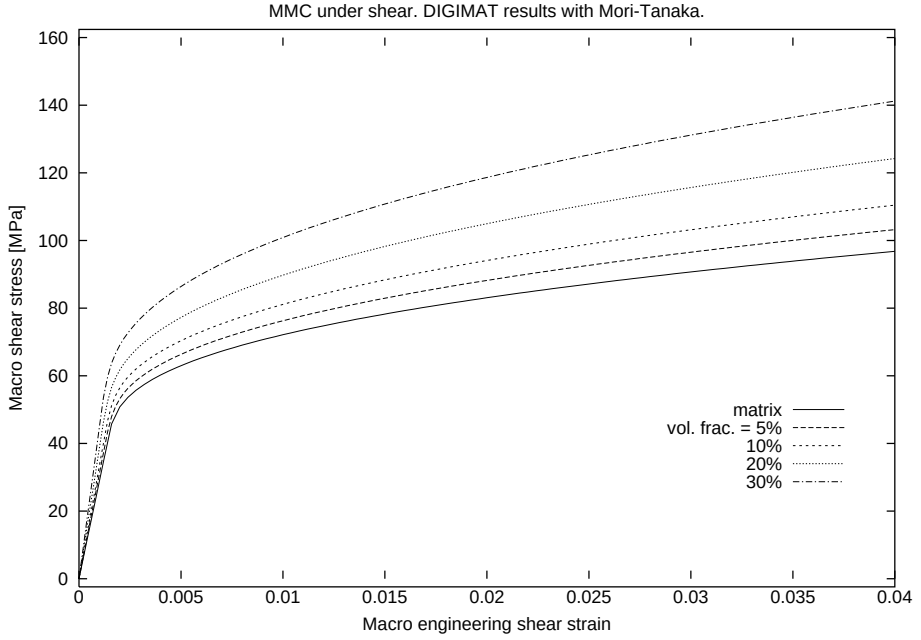

Fig. 8. MMC under macro-shear strain (macro-plane stress). MT predictions for various values of inclusions' volume fraction v_1.

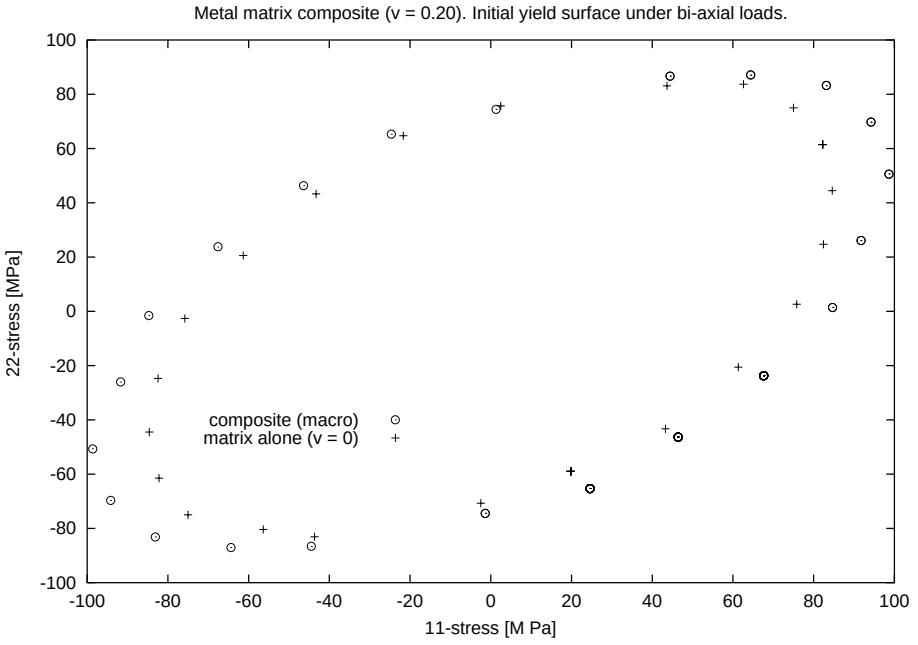

Fig. 9. MMC ($v_1 = 20\%$): MT prediction of initial yield surface for proportional bi-axial macro-strains under macro-plane stress conditions.

difference between MT and DI predictions for high values of v_1 is more pronounced than for MMC (the stiffness ratio E_1/E_0 of the two phases is 23.13 for PMC and 5.33 for MMC).

Figs. 11 and 12 show the results of macro-tension tests under imposed macro-strain. Our MT results are compared against those of Tandon and Weng (1988) in Fig. 11 and excellent agreement is found. In Fig. 12, our MT predictions are plotted against experimental data, and as in (Tandon and Weng, 1988) an excellent match is found in all cases except $v_1 = 0.52$.

In Fig. 13, for $v_1 = 42\%$, a cyclic tension/compression test under imposed macro-strain (peak values: $\pm 4\%$) is simulated with three methods: MT, DI and FE. In the first monotonic phase of the loading history, it seen that DI agrees perfectly with FE for the linear elastic response, but predicts an overly stiff plastic response. The MT model, however, gives a poor prediction of the elastic stiffness but a satisfying simulation of the plastic response. This observation continues to hold for the subsequent phases of the loading, and overall MT predicts the plastic response much better than DI. We have done similar simulations for all other values of v_1 and the conclusions are the same. Again, note that the secant formulation is *not* able to simulate cyclic plasticity, since in essence it is a non-linear elastic formulation.

Finally, macro-shear tests were simulated and the results obtained with MT are plotted in Fig. 14.

9.4. Chaboche's cyclic plasticity model

The matrix material considered in this section is a low-carbon (AISI 1010) steel. The experimental data were first identified with Chaboche's cyclic plasticity model with the parameter values reported in (Doghri, 1993): $E_0 = 210$ GPa, $\nu_0 = 0.3$, $\sigma_Y = 200$ MPa, exponential-law isotropic hardening with saturation ($R(p) = R_\infty[1 - \exp(-mp)]$) with $R_\infty = 2$ GPa and $m = 0.26$, non-linear kinematic hardening with parameters $a = 17$ GPa and $b = 21$.

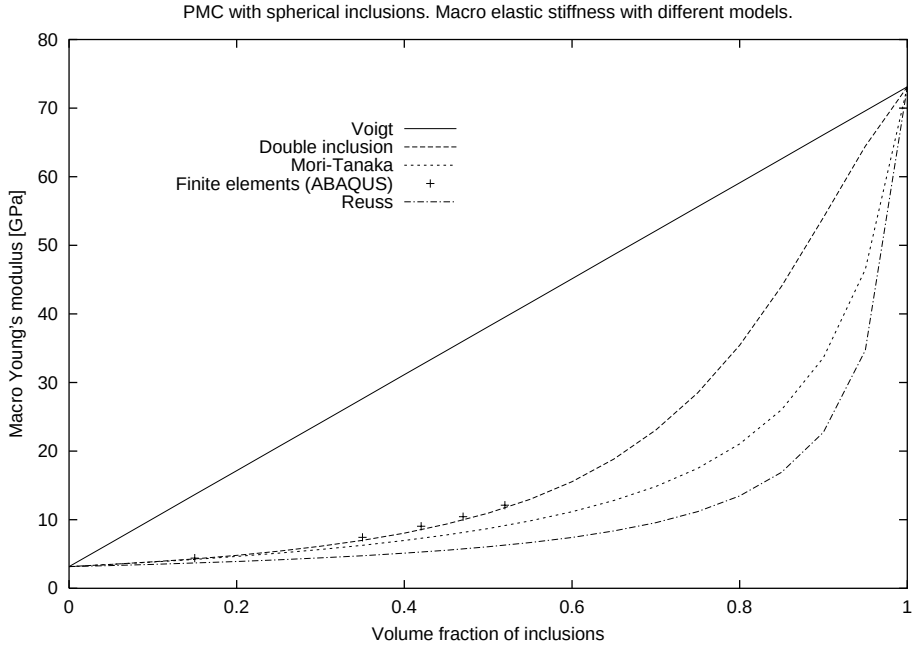

Fig. 10. PMC: macro-Young's modulus predictions with different models: (1) Voigt (uniform strain), (2) double inclusion, (3) Mori–Tanaka, (4) finite elements (unit cell) and (5) Reuss (uniform stress).

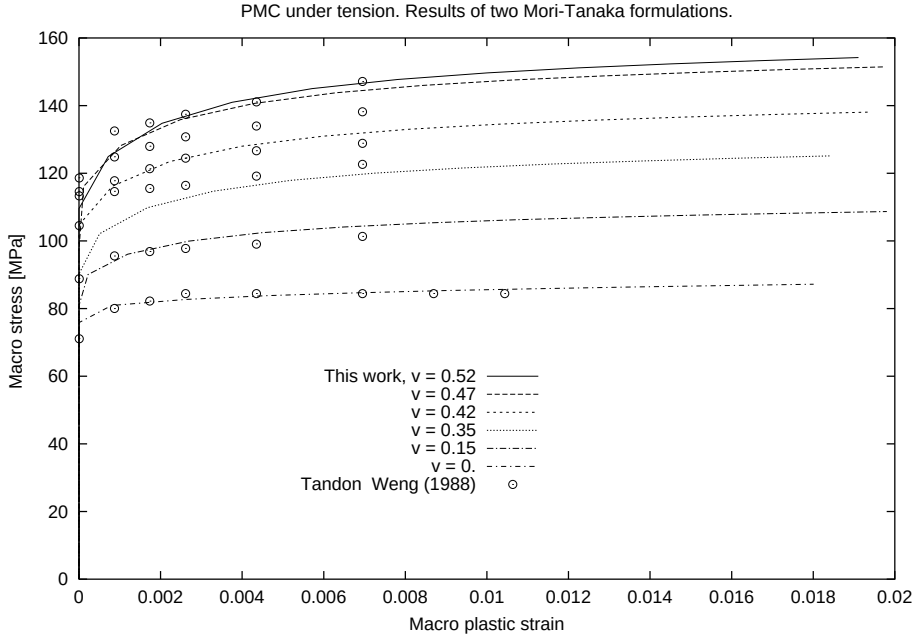

Fig. 11. PMC under macro-tension for various values of inclusions' volume fraction v_1. Predictions obtained with two MT formulations: (1) incremental (this work) and (2) secant (Tandon and Weng, 1988).

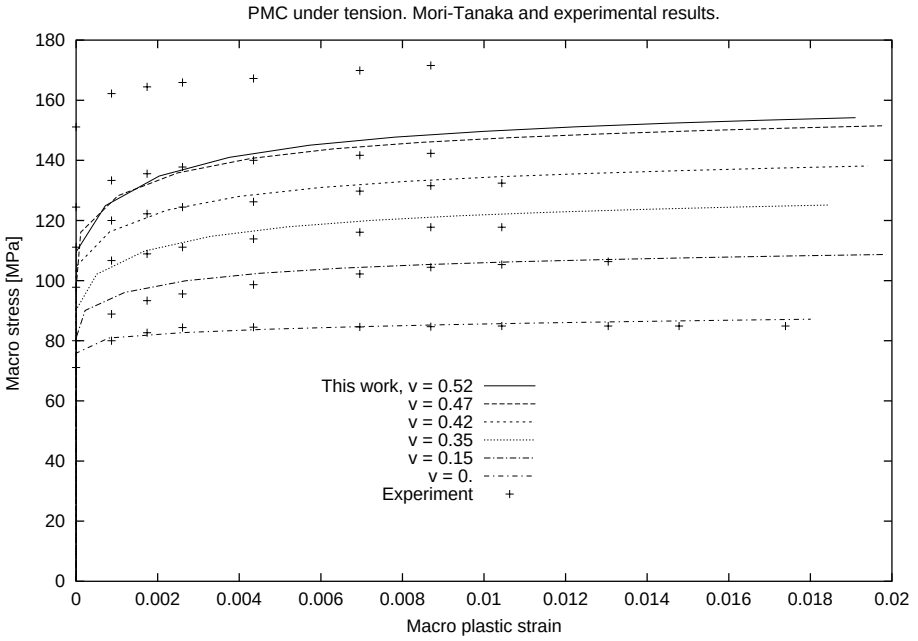

Fig. 12. PMC under macro-tension for various values of inclusions' volume fraction v_1. Comparison between: (1) predictions obtained with Mori–Tanaka (this work) and (2) experimental results.

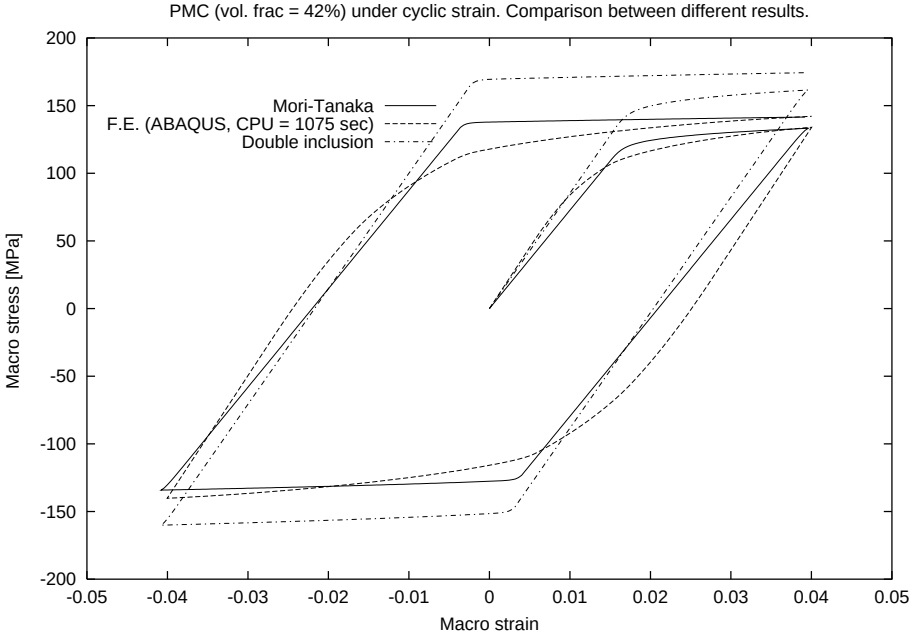

Fig. 13. PMC ($v_1 = 42\%$) under cyclic macro-strain (macro-uniaxial stress). Comparaison of different predictions: (1) MT model, (2) finite elements (unit cell) and (3) interpolative double inclusion model.

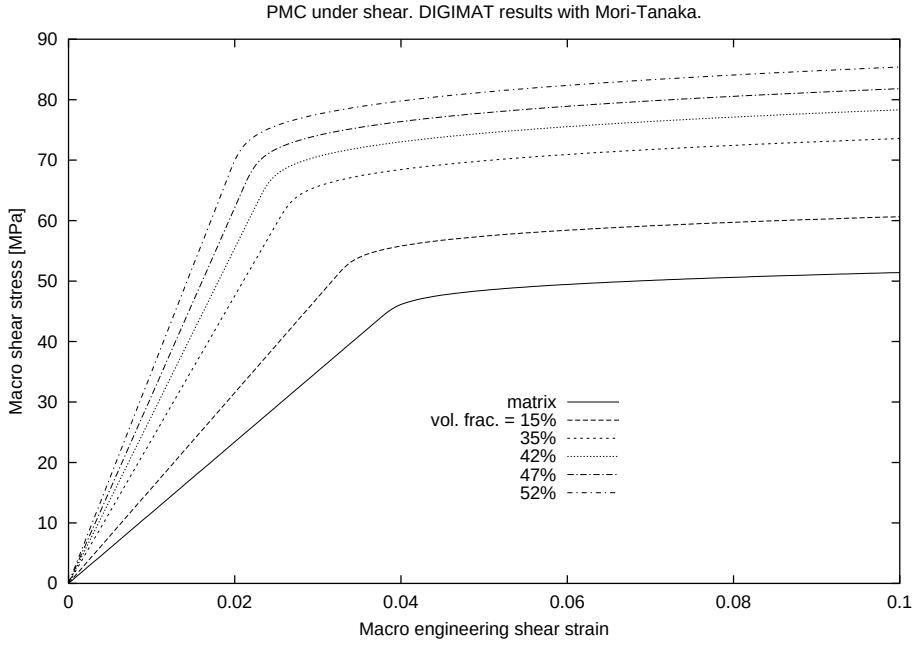

Fig. 14. PMC under macro-shear strain (macro-plane stress). MT predictions for various values of inclusions' volume fraction v_1.

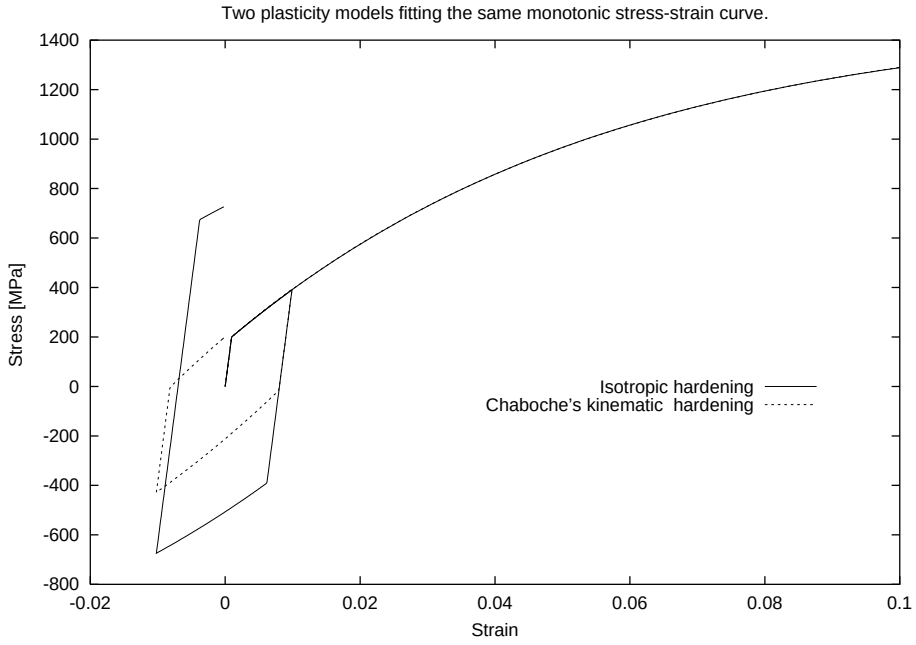

Fig. 15. Two plasticity models, one with isotropic hardening only and the other with combined non-linear isotropic and kinematic hardenings (Chaboche's model). The two models fit the same monotonic stress–strain curve up to 10% strain, but their responses differ under cyclic load history (results for $\pm 1\%$ cyclic strain shown).

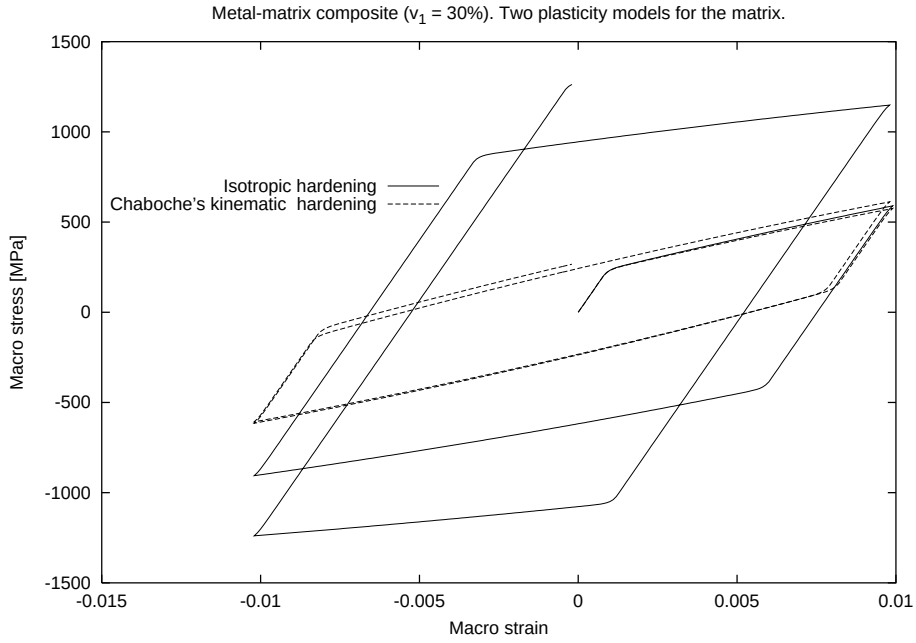

Fig. 16. MMC ($v_1 = 30\%$) under cyclic macro-strain (macro-uniaxial stress). MT predictions using two plasticity models fitting the same monotonic stress–strain curve of the matrix: (1) isotropic hardening only and (2) non-linear isotropic and kinematic hardenings (Chaboche's model).

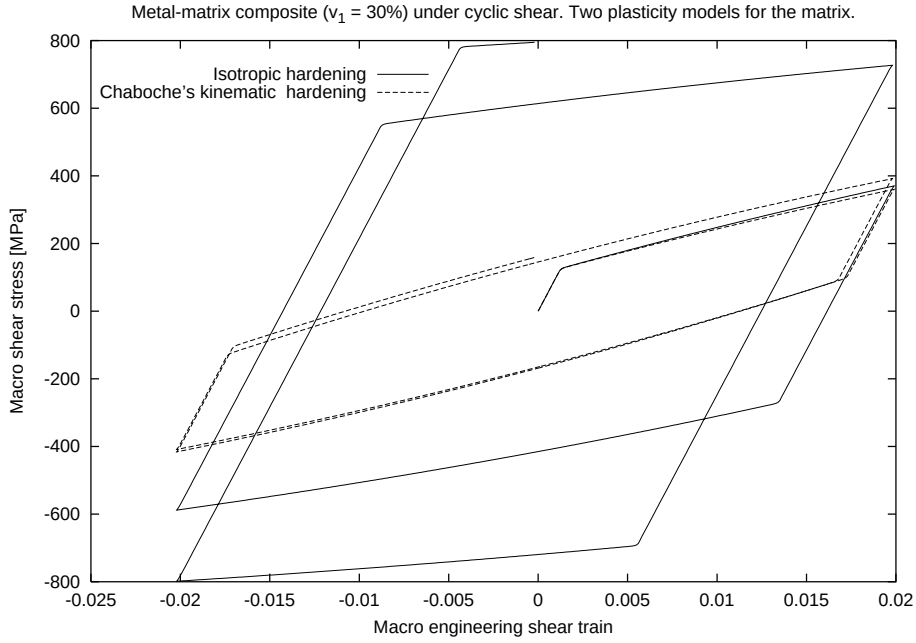

Fig. 17. MMC ($v_1 = 30\%$) under cyclic macro-shear strain (macro-plane stress). MT predictions using two plasticity models fitting the same monotonic stress–strain curve of the matrix: (1) isotropic hardening only and (2) non-linear isotropic and kinematic hardenings (Chaboche's model).

Next, the matrix material was modeled with classical J_2 elasto-plasticity (no kinematic hardening) and a new set of parameters was identified so that to obtain the *same* stress–strain curve in a monotonic tension test up to 10% of total strain. The following parameters were found for isotropic hardening with saturation (the values of E_0, v_0 and σ_Y are unchanged): $R_\infty = 1286.68$ MPa and $m = 19.9325$.

Fig. 15 shows that the monotonic responses of the two models up to 10% strain are indeed identical. However, for a cyclic tension/compression test under imposed strain (peak values $\pm 1\%$), it is seen in Fig. 15 that upon unloading and re-entry into plasticity, the answers become very different as Chaboche's model predicts a Baushinger effect while classical J_2 finds opposite yield stresses in tension and compression.

A hypothetical composite was designed by reinforcing the matrix with spherical elastic ceramic inclusions ($E_1 = 400$ GPa and $v_1 = 0.2$).

Results of macro-uniaxial tension/compression of the composite ($v_1 = 30\%$) are shown in Fig. 16 using MT and the two material models for the matrix discussed above. Remarks made for the matrix alone (Fig. 15) hold for the composite (Fig. 16).

The same composite was simulated under macro-cyclic shear and the results are plotted in Fig. 17. Again, the results and the comments are similar to those of Figs. 15 and 16.

10. Two-scale numerical simulations of composite structures

10.1. General considerations

We integrated our homogenization code DIGIMAT into the FE program ABAQUS through its user-defined material interface UMAT. We adopted the following *two-scale* approach. A classical FE analysis is carried out at macro-scale, and for each time interval $[t_n, t_{n+1}]$ and each iteration of the global equilibrium equations at macro-scale, and at each quadrature point of the macro-FE mesh, the homogenization module UMAT/DIGIMAT is called. The data that are passed to it by ABAQUS are the total macro-strains $\overline{\boldsymbol{\epsilon}}_n$ and $\overline{\boldsymbol{\epsilon}}$ (as well as material constants and history information at t_n). The DIGIMAT code returns the macro-stress $\overline{\boldsymbol{\sigma}}$ and macro-tangent moduli $\overline{\boldsymbol{c}}$ at t_{n+1}. The microstructure is not "seen" by ABAQUS but only by DIGIMAT, which considers each quadrature point to be the center of a RVE which contains the heterogeneous microstructure.

As we shall see in the next subsections, this two-scale procedure allows to compute structures made of composite materials within reasonable CPU time and memory usage on an ordinary workstation. The results prove that the whole procedure converges and does so rapidly. The procedure is comprised of the following algorithms:

(i) The homogenization algorithms (Sections 7.2 and 8.2), with as a subset the algorithms for elasto-plasticity (time-integration and computation of consistent moduli).
(ii) The algorithm for macro-stress constraints (Section 6.4) because the two examples use shell elements which must satisfy macro-plane stress conditions.
(iii) The FE computations at macro-scale. The results show that the macro-tangent moduli $\overline{\boldsymbol{c}}$ and the macro-stresses $\overline{\boldsymbol{\sigma}}$ which are returned by the homogenization module DIGIMAT/UMAT allow ABAQUS to converge rapidly to a solution in the FE sense.

Finally, we point out that our homogenization-based approach gives results with acceptable accuracy while being much cheaper than a direct method (FE computations at macro- and micro-scales) on all aspects: CPU time, memory usage and user time.

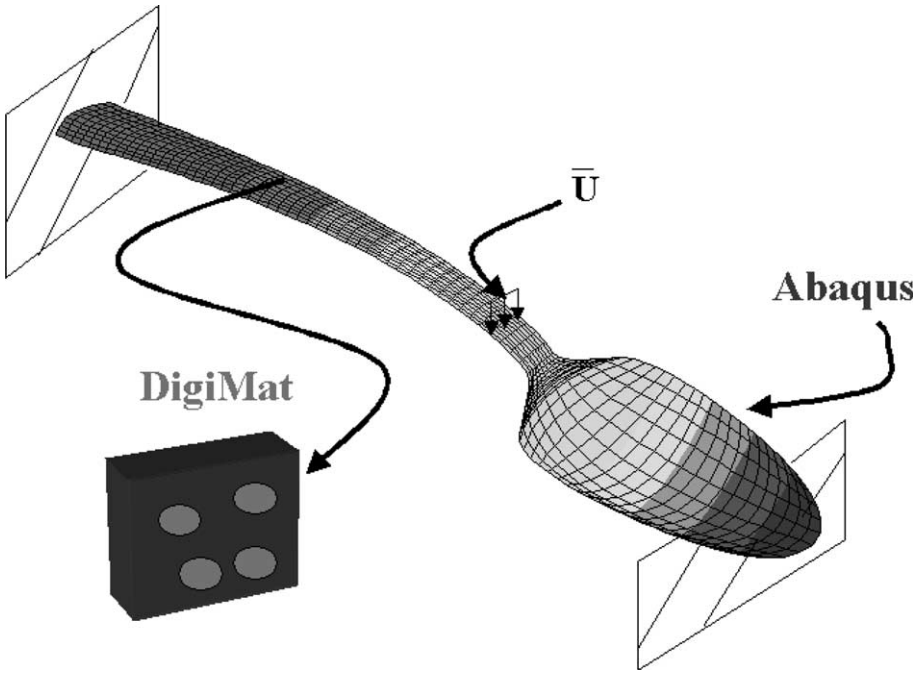

Fig. 18. MMC spoon built-in at both ends, under cyclic displacement at mid-span. Two-scale procedure: FE program ABAQUS at macro-scale and homogenization code DIGIMAT at micro-scale (with an instantaneous UMAT interface between ABAQUS and DIGIMAT).

10.2. MMC spoon under cyclic bending

A spoon made of the MMC material of Section 9.2 is built-in at both ends and subjected to a cyclic displacement (peak values ± 4 mm) at mid-span, see Fig. 18. The mesh used 800 shell elements of type S4R5 and 891 nodes.

The load–displacement curves are shown in Fig. 19 for two cases: a homogeneous matrix material (ABAQUS alone) and the composite material ($v_1 = 30\%$, ABAQUS with UMAT/DIGIMAT interface). The effect of the reinforcing phase on the overall response of the structure is obtained in a very cost-effective way: the two-scale approach only takes 2889 s of CPU time on an average Compac (ex-Digital) DEC Alpha workstation, and this is just 3.95 times more expensive than the homogeneous case.

10.3. PMC bottle under cyclic torsion

A bottle made of the PMC material of Section 9.3 is built-in at one end and subjected to cyclic torsion under imposed axial rotation at the other end (peak values ± 0.5 rad), see Fig. 20. The mesh used 3290 shell elements of type S4R and 3292 nodes.

The torque–rotation curves are shown in Fig. 21 for two cases: a homogeneous matrix material (ABAQUS alone) and the composite material ($v_1 = 42\%$, ABAQUS with UMAT/DIGIMAT interface). The two-scale computation only takes 3980 s of CPU time on the same Compac DEC Alpha workstation, and this is only 3.44 times the CPU cost of the homogeneous calculation.

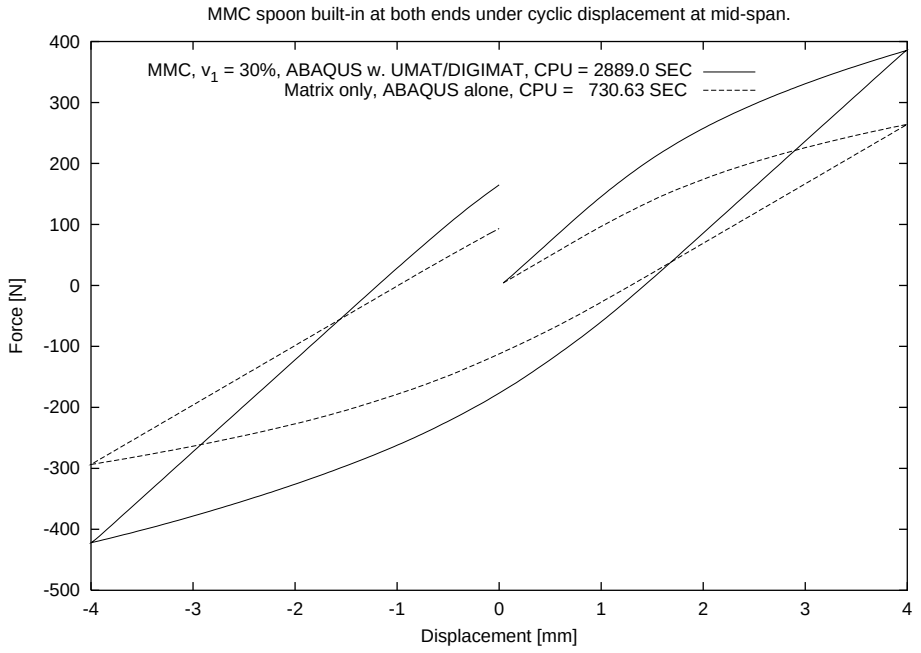

Fig. 19. MMC spoon built-in at both ends, under cyclic displacement at mid-span. Force–displacement curves in two cases: (1) composite ($v_1 = 30\%$) using a two-scale procedure with an instantaneous UMAT interface between FE program ABAQUS and homogenization code DIGIMAT (with MT model) and (2) matrix only material ($v_1 = 0$) with ABAQUS.

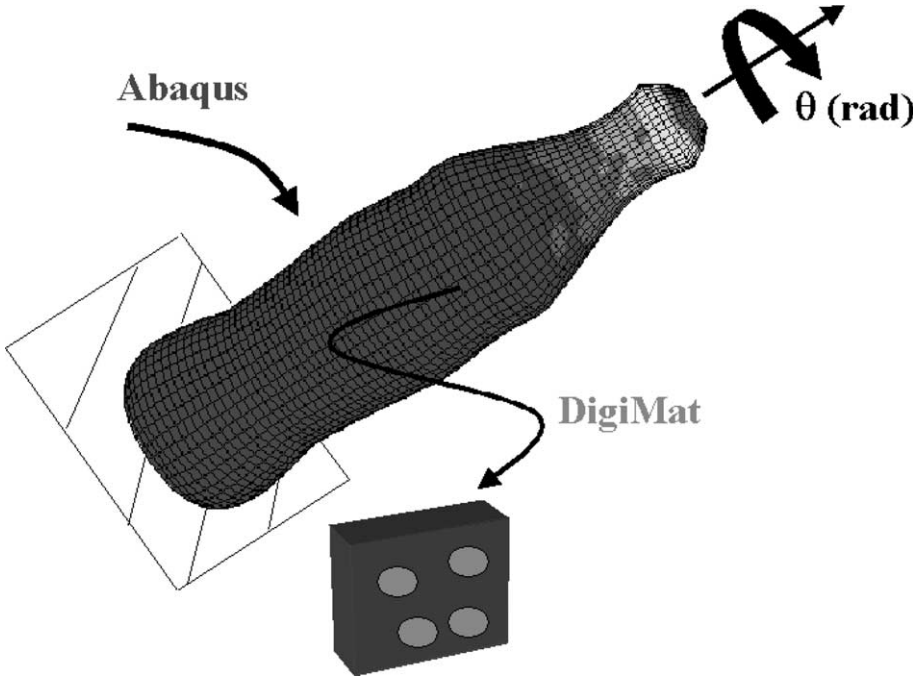

Fig. 20. PMC bottle under cyclic torsion. Two-scale procedure: finite element program ABAQUS at macro-scale and homogenization code DIGIMAT at micro-scale (with an instantaneous UMAT interface between ABAQUS and DIGIMAT).

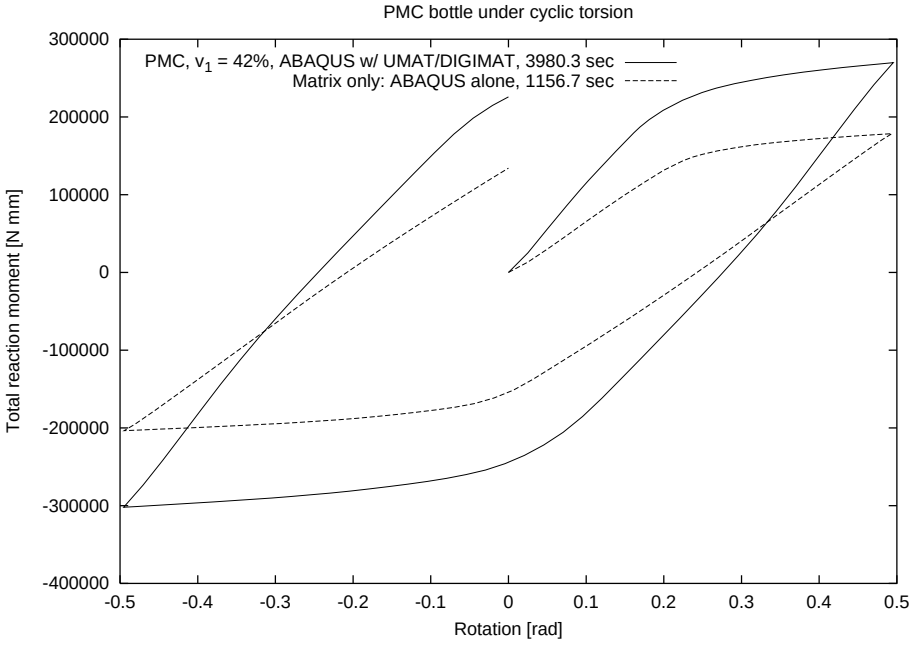

Fig. 21. PMC bottle under cyclic torsion. Moment–rotation curves in two cases: (1) composite ($v_1 = 42\%$) using a two-scale procedure with an instantaneous UMAT interface between FE program ABAQUS and homogenization code DIGIMAT (with MT model) and (2) matrix only material ($v_1 = 0$) with ABAQUS.

11. Conclusions and future work

In this paper, we studied micro/macro-modeling and numerical simulation of two-phase elasto-plastic composite materials and structures.

We extended to non-linear, rate-independent models two homogenization schemes: MT and a DI. The latter is Lielens' version (Chapter 9 in (Lielens, 1999)) of the original Nemat-Nasser and Hori (1999, Section 10).

The extension of homogenization schemes is based on a Hill-type incremental formulation which allows the simulation of unloading and cyclic loadings.

The formulation allows to handle any rate-independent model for each phase. It was tested with two different material models: classical J_2 elasto-plasticity and Chaboche's model with non-linear kinematic and isotropic hardenings.

We studied the crucial issue of tangent moduli: elasto-plastic (or "continuum") versus algorithmic (or "consistent"), and anisotropic versus isotropic. We applied two methods of extraction of isotropic parts of anisotropic operators. We compared mathematically the stiffnesses of various tangent moduli, as this might give an explanation for the overall predictions obtained when Eshelby's tensor is computed with anisotropic (continuum or consistent) or isotropic moduli.

All rate equations were discretized in time using implicit schemes at two levels: (i) the constitutive models and (ii) the homogenization schemes. In the latter case, we showed the importance of the time-integration parameter (α) on the accuracy of the overall response. The results that we reported in this paper were all obtained with $\alpha = 1/2$ (mid-point rule) or $\alpha = 2/3$.

We tested the robustness of the formulation and its implementation by considering at least two composites with completely different properties: a MMC and a PMC, and running several discriminating numerical simulations: cyclic macro-tension/compression, cyclic macro-shear and macro-bi-axial loadings.

In many cases, the results were compared with those of direct computations in which the BVP for each RVE is solved directly using FEs. For MMC, our results were also compared to predictions obtained with other formulations and reported in (Segurado et al., 2002), namely: 3D FE simulations, a classical secant MT formulation and Suquet's formulation where reference materials are defined with the phase-averages of the second-order moments of stress. Good agreement was found between our predictions and the 3D FE targets, and the accuracy increases with increasing hardening.

The results showed that DI gives an excellent prediction of the elastic stiffness but that the plastic response is generally better predicted by MT.

Finally, our homogenization code DIGIMAT was integrated into the FE program ABAQUS using a user material interface UMAT. A two-scale method was used: a FE model at macro-scale, and at each quadrature point of the macro-FE mesh, the homogenization module UMAT/DIGIMAT is called. The procedure allows to compute real-life structures made of composite materials within reasonable CPU time and memory usage. Two examples were shown: a MMC spoon built-in at both ends and subjected to cyclic bending and a PMC bottle under cyclic torsion.

The results reported in this paper are based on two assumptions: (1) reference moduli are computed with average strains in each phase; and (2) Eshelby's tensor is computed with an isotropic part of the reference matrix moduli.

Although good results were obtained, there is a need for a better understanding of the two issues, and it would be interesting to implement some other proposals from the literature and compare their predictive capabilities.

This paper only dealt with rate-independent small-strain composite materials, with inclusions having the same shape, material properties and orientation. Numerical results were only presented for spherical inclusions.

Firstly, we are currently studying the influence of the shape and orientation of inclusions on the overall properties of two-phase elasto-plastic composites (Friebel, 2002; Doghri and Friebel, 2003).

Secondly, we intend to extend the formulation and algorithms to finite-strain elasto-plastic composites. Hill (1972) and Nemat-Nasser (1999) showed that the finite-strain formulation follows the same lines as the infinitesimal-strain case provided that one uses the following ingredients: (i) work with the reference configuration; (ii) use the nominal stress $\boldsymbol{P}^{\mathrm{T}}$ as a stress measure; (iii) use the rate of deformation gradient $\dot{\boldsymbol{F}}$ as a strain rate measure.

Thirdly, we will turn our attention to elasto-viscoplastic composites. The earlier formulations of Hutchinson (1976) and Molinari et al. (1987), although successful, are based on several restrictive assumptions. We are looking for a general formulation which would work with any elasto-viscoplastic model under general loadings (including cyclic ones). With this perspective, it seems worthwhile to investigate the recent proposal of Masson et al. (2000). In the authors' so-called "affine method", homogenization models are formulated using instantaneous "linear thermoelastic" solids.

Acknowledgements

A. Ouaar acknowledges an assistantship from UCL and partial support of the IUAP P5/08 project "From microstructure towards plastic behaviour of single- and multi-phase materials" of the Federal Office for Scientific, Technical and Cultural Affairs, Belgian State Prime Minister's Office. The authors are grateful to F. Lani, G. Lielens and T. Pardoen for helpful discussions.

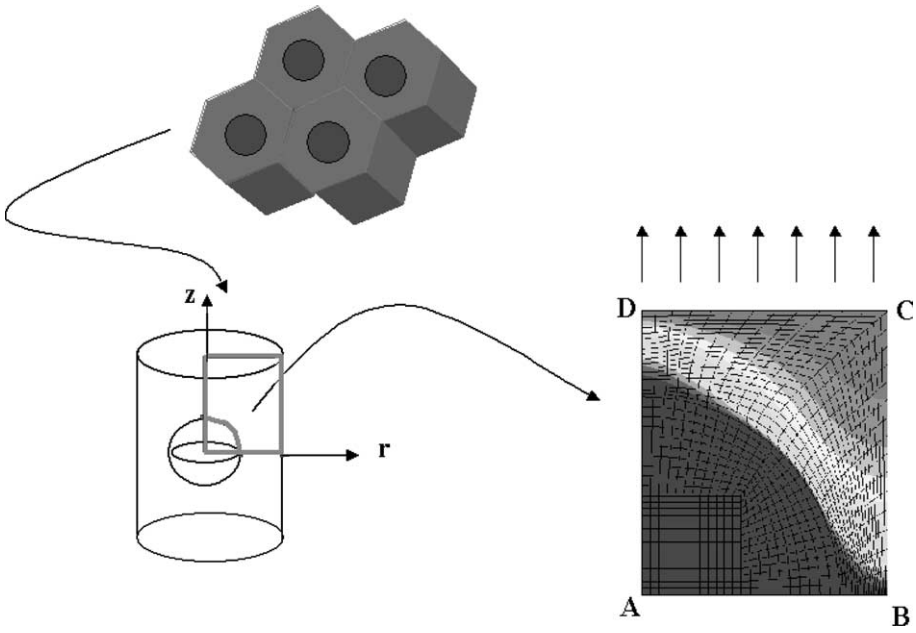

Fig. 22. Unit cell used for FE computations assuming a periodic microstructure and axisymmetric loadings.

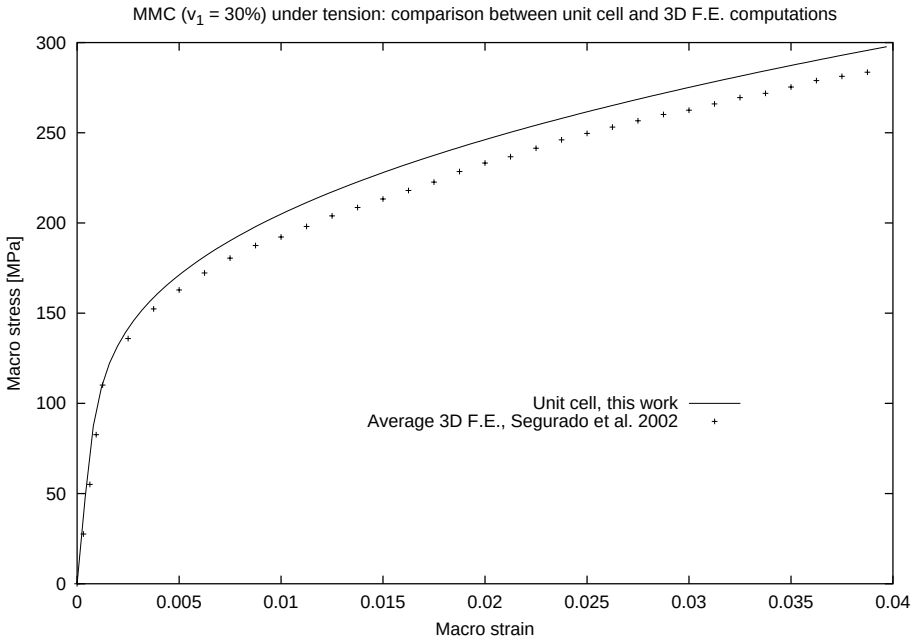

Fig. 23. MMC ($v_1 = 30\%$) under macro-tension. Comparaison of finite element results obtained with two models: (1) a unit cell assuming a periodic microstructure (this work) and (2) average 3D FE computations of a RVE containing randomly located spheres (Segurado et al., 2002).

Appendix A. Unit cell for FE computations

Some macro-tension/compression results were validated against FE computations of a unit cell, assuming that the composite has a periodic microstructure with a square arrangement. The cell has a plane geometry in the (r,z) plane, where r is the radial coordinate and z the coordinate along the symmetry axis. The cell geometry is shown in Fig. 22; z- and r-coordinate lines correspond to vertical and horizontal segments, respectively. Along the symmetry axis (left vertical segment DA), radial displacement is zero. Along the bottom horizontal line AB, the vertical displacement is zero. Vertical displacements are imposed on the top horizontal side CD while the right vertical side BC is constrained to have the same radial displacement. The mesh used 3002 nodes and 963 ABAQUS axisymmetric CAX8R elements.

For the MMC studied in Section 9.2 (with $v_1 = 30\%$) a macro-tension test was simulated in (Segurado et al., 2002) by performing 3D FE computations on a cube containing 30 spheres. A typical mesh contained about 60,000 elements and 90,000 nodes. Twelve meshes were generated corresponding to different arrangements of the spheres and BCs and the average response is plotted in Fig. 23, together with the FE curve obtained with our unit cell. The figure shows that the unit cell over-predicts the macro-response by comparison with the more accurate 3D FE computations on a cubic RVE containing many spheres without a periodic distribution.

References

ABAQUS, a general-purpose finite element program, Hibbitt, Karlsson & Sorensen, Inc., Pawtucket, RI, USA, 2001.

Armstrong, P.J., Frederick, C.O., 1966. A mathematical representation of the multiaxial Baushinger effect. Report no. RD/B/N731, General Electricity Generating Board, Berkeley Nuclear Laboratoires.

Benveniste, Y., 1987. A new approach to the application of Mori-Tanaka's theory in composite materials. Mech. Mater. 6, 147–157.

Bornert, M., Bretheau, T., Gilormini, P., (Eds.) 2001a. Homogénéisation en mécanique des matériaux, 1. Matériaux aléatoires élastiques et milieux périodiques. HERMES Science, Paris, 2001.

Bornert, M., Bretheau, T., Gilormini, P., (Eds.) 2001b. Homogénéisation en mécanique des matériaux, 2. Comportements non linéaires et problèmes ouverts, HERMES Science, Paris, 2001.

Doghri, I., 1993. Fully implicit integration and consistent tangent modulus in elastoplasticity. Int. J. Numer. Meth. Engng. 36, 3915–3932.

Doghri, I., 2000. Mechanics of Deformable Solids- Linear, Nonlinear, Analytical and Computational Aspects. Springer-Verlag, Berlin.

Doghri, I., Friebel, C., 2003. Effective elasto-plastic properties of inclusion-reinforced composites. Study of shape, orientation and cyclic response, in preparation.

Eshelby, J.D., 1957. The determination of the elastic field of an ellipsoidal inclusion, and related problems. Proc. Roy. Soc. London Ser. A 241, 376–396.

Friebel, C., 2002. Modélisation et simulation micro-macro de matériaux composites. Etude de l'influence des renforts (matériau, forme et orientation). Graduation report in applied mathematics, UCL/FSA, Louvain-la-Neuve, Belgium.

Gavazzi, A.C., Lagoudas, D.C., 1990. On the numerical evaluation of Eshelby's tensor and its application to elastoplastic fibrous composites. Comput. Mech. 7, 13–19.

Gonzalez, C., Llorca, J., 2000. A self-consistent approach to the elasto-plastic behaviour of two-phase materials including damage. J. Mech. Phys. Solids 48, 675–692.

Hashin, Z., Shtrikman, S., 1963. A variational approach to the theory of the elastic behaviour of multiphase materials. J. Mech. Phys. Solids 11, 127–140.

Hill, R., 1965. A self-consistent mechanics of composite materials. J. Mech. Phys. Solids 13, 213–222.

Hill, R., 1972. On constitutive macro-variables for heteregeneous solids at finite strain. Proc. R. Soc. London A 326, 131–147.

Hutchinson, J.W., 1976. Bounds and self-consistent estimates for creep of polycrystalline materials. Proc. Roy. Soc. London. A 348, 101–127.

Kouznetsova, V., Geers, M.G.D., Brekelmans, W.A.M., 2002. Multi-scale constitutive modeling of heterogeneous materials with a gradient-enhanced computational homogenization scheme. Internat. J. Numer. Meth. Engng. 54, 1235–1260.

Lemaitre, J., Chaboche, J.-L., 1998. Mechanics of Solid Materials. Cambridge University Press, England.

Lielens, G., 1999. Micro-macro modeling of structured materials. Ph.D. dissertation, UCL/FSA, Louvain-la-Neuve, Belgium.

Masson, R., Bornert, M., Suquet, P., Zaoui, A., 2000. An affine formulation for the prediction of the effective properties of nonlinear composites and polycrystals. J. Mech. Phys. Solids 48, 1203–1227.

Molinari, A., Canova, G.R., Ahzi, S., 1987. A self-consistent approach of the large deformation polycrystal viscoplasticity. Acta Metall. 35 (12), 2983–2994.

Mori, T., Tanaka, K., 1973. Average stress in matrix and average elastic energy of materials with misfitting inclusions. Acta Metall. 21, 571–574.

Mura, T., 1987. Micromechanics of Defects in Solids, second ed. Martinus Nijhoff Publishers, Dordrecht, The Netherlands.

Nemat-Nasser, S., 1999. Averaging theorems in finite deformation plasticity. Mech. Mater. 31, 493–523.

Nemat-Nasser, S., Hori, M., 1999. Micromechanics: Overall Properties of Heterogeneous Materials, second ed. Elsevier Science publishers, Amsterdam.

PALMYRA, 2001. A finite-element software for heterogeneous micro-structures. Materials Simulation GmbH, Zurich, Switzerland.

Pettermann, H.E., Planskensteiner, A.F., Bohm, H.J., Rammerstorfer, F.G., 1999. A thermo-elasto-plastic constitutive law for inhomogeneous materials based on an incremental Mori–Tanaka approach. Comput. Struct. 71, 197–214.

Ponte Castañeda, P., 1996. Exact second-order estimates for the effective mechanical properties of nonlinear composite materials. J. Mech. Phys. Solids 44 (6), 827–862.

Ponte Castañeda, P., Suquet, P., 1998. Adv. Appl. Mech. 34, 171–302.

Ponte Castañeda, P., Suquet, P., 2001. Nonlinear composites and microstructure evolution. In: Mechanics for a New Millenium, Proceedings of ICTAM 2000-Chicago. Kluwer Academic Publishers, Dordrecht, The Netherlands, pp. 253–273.

Segurado, J., Llorca, J., Gonzalez, C., 2002. On the accuracy of mean-field approaches to simulate the plastic deformation of composites. Scr. Mater. 46, 525–529.

Simo, J.C., Taylor, R.L., 1985. Consistent tangent operators for rate-independent elastoplasticity. Comput. Meth. Appl. Mech. Engng. 48, 101–118.

Suquet, P., (Ed.), 1997. Continuum micromechanics, CISM Lecture notes, Udine, Italy, Springer-Verlag, Berlin, 1997.

Tandon, G.P., Weng, R.L., 1988. A theory of particle-reinforced plasticity. J. Appl. Mech. Trans. ASME 55, 126–135.